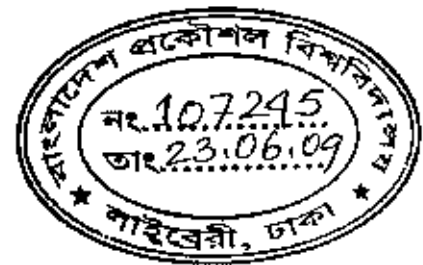


**TRANSPORT AND MAGNETIC PROPERTIES OF MAGNETICALLY
ORDERED $(\text{Fe}_{100-x}\text{V}_x)_{75}\text{P}_{15}\text{C}_{10}$ AMORPHOUS ALLOYS**

by

Md. Golam Mertoza Hossain

*A dissertation submitted in partial fulfillment of the requirement for the degree of M.Phil. in
the department of Physics, Bangladesh University of Engineering and Technology,
Dhaka-1000*



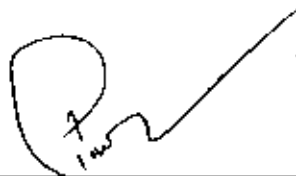
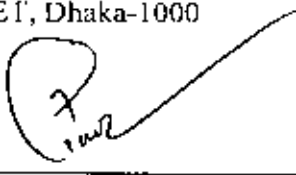
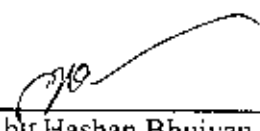


**Department of Physics
Bangladesh University of Engineering and Technology
Dhaka-1000, Bangladesh
March 2009**



Certification of thesis work

The thesis titled "*Transport and Magnetic Properties of Magnetically Ordered (Fe_{100-x}V_xP₁₅C₁₀ Amorphous Alloys*", submitted by **Md. Golam Mortoza Hossain**, Roll No.: 040314034F, Session-April 2003, has been accepted as satisfactory in partial fulfillment of the requirement for the degree of **Master of Philosophy (M. Phil.)** in Physics on 31 March, 2009.

BOARD OF EXAMINERS

1. 
Dr. Md. Feroz Alam Khan (Supervisor)
Professor, Department of Physics
BUET, Dhaka-1000
Chairman
2. 
Dr. Md. Feroz Alam Khan
Professor and Head, Department of Physics
BUET, Dhaka-1000
Member [Ex-Officio]
3. 
Dr. Md. Abu Hashan Bhuiyan
Professor, Department of Physics
BUET, Dhaka-1000
Member
4. 
Dr. Md. Mostak Hossain
Associate Professor, Department of Physics
BUET, Dhaka-1000
Member
5. 
Dr. Mokbulur Rahman
Professor, Department of Physics
University of Dhaka, Dhaka-1000
Member (External)

Candidate's Declaration

It is hereby declared that this thesis or any part of it has not been submitted elsewhere for the award of any degree or diploma.



(Md. Golam Mertoza Hossain)

Candidate

Roll No.: 040314034F

Session: April-2003

Acknowledgements

I am extremely delighted to express my indebtedness and a deep gratitude to my reverend teacher **Dr. Md. Feroz Alam Khan**, Professor & Head, Department of Physics, Bangladesh University of Engineering and Technology, Dhaka. for his supervision, guidance, valuable suggestion and inspiration which allowed me to complete this thesis.

I am also thankful to all other teachers of the department of Physics, BUET specially Professor Dr. Mominul Huq, Professor Dr. Abu Hashan Bhuiyan, Professor Dr. Nazma Zaman, Professor Jiban Poddar, Dr. Mostak Hossain, Dr. A.K.M Akther Hossain, Dr. Nazrul Islam. Mrs. Afia Begum, Mr. Md. Rafi Uddin, Mrs Nasreen Akther. Mr. Md Abdul Basith, Muhammad Samir Ullah and Mohammad Abu Sayem for their encouragement and help during my research work.

I would like to thank Dr. Md. Abdul Gafur, Sr. Engineer, PP & PDC, Mr. Jasim Uddin Khan, Scientific Officer, BCSIR, Dhaka, for their invaluable contributions on this research work.

Sincere and deepest thanks to my friends A.K.M Shafiqullah, Md. Quamruzzaman, Md. Nurul Huda, Supria Chowdhury, Subhasish Sardar, M Amirul Islam for their friendship and support. I also give thanks to other M.Phil students of BUET for their kind help and inspirations. Thanks are given also to all staff members of the Department of Physics, BUET for giving incredible support to my research work.

I am also thankful to M. Kamruzzaman, an M.Phil student of BUET for his assistance during my experimental work.

I expressed my gratitude to my Parents, brothers & sister, Father-in-law and Mother-in-law, brother-in-law and specially my wife for their encouragement in keeping my spirit high.

I also want to express my gratefulness to the authority of BUET for giving me the opportunity to do this research work and financial support.

Finally, I would like to express my gratitude to Almighty Allah whose mercy helped me all time.

CONTENTS

i.	Certification	i
ii	Dedication	ii
iii.	Declaration	iii
iv	Acknowledgement	iv
v.	Contents	v
vi	Abstract	viii
Chapter One : Introduction		
1.1	Introduction	2
1.2	Aim of this Work	4
Chapter Two : Preparation of Amorphous Ribbons		
2.1	Introduction	7
2.2	Conditions to be prepared amorphous materials	8
2.3	Preparation technique of amorphous ribbon	8
2.3.1	The atomic deposition methods	8
2.3.2	The fast cooling of the melt	8
2.3.2.1	The Melt Spinning Technique	9
2.4	Experimental details for the preparation of amorphous ribbon	10
2.5	Factors contributing to glass formation	11
Chapter Three : Theoretical Perspective		
3.1	DC Electrical Resistivity	14
3.1.1	Electrical Resistivity	17
3.2	Magnetoresistance	18
3.3	Impedance and the phases	20
3.4	Inductive Reactance	21
3.5	Inductance	22
3.6	Permeability	22
3.7	Heat Diffusivity	24
3.8	Differential Thermal Analysis (DTA)	24
3.8.1	The endothermic and exothermic reactions	25

3.8.2	Exothermic reaction	25
3.8.3	Peak Area, Peak Temperature, Effect of heating rate	26
3.8.4	Peak area function	26
3.8.5	Effect of heating rate	28
3.8.6	Transition state	28
3.8.7	Activation Energy E_{act}	28
3.8.8	Change of Phase	29
3.8.9	The latent heat in phase changes	29
3.8.10	Entropy and Disorder	29
3.8.11	Experimental set-up of the DTA apparatus	31
3.8.11.1	Sample Holder	31
3.8.11.2	Thermocouples	31
3.8.11.3	Furnace	32
3.8.11.4	Temperature Controller	32
3.8.11.5	Recorder	32
3.9	Thermo Gravimetric Analysis (TGA)	32
3.10	Differential Thermo Gravimetric (DTG)	33
3.11	Scanning Electron Microscopy	33
3.11.1	Working Function of SEM	34
3.11.2	Topography	36
3.11.3	Morphology	36
3.11.4	Composition	36
3.11.5	Crystallographic Information	36
3.12	Working Principle of Vibrating Sample Magnetometer (VSM)	36
Chapter Four : Experimental Techniques		
4.1	Techniques for DC electrical measurement with magnetic field	39
4.1.1	DC electrical resistivity: 2-probe and 4-probe method	39
4.1.2	The Van der Pauw method	42
4.2	Impedance and Permeability measurement	44
4.3	Heat Diffusivity measurement	44
4.4	Scanning Electron Microscope	46
4.5	DTA, TGA and DTG measurement	46

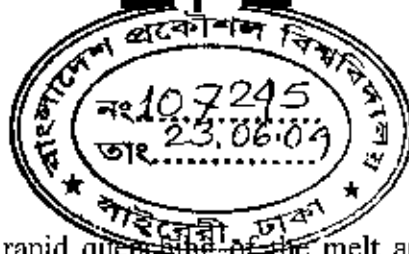
Chapter Five : Results and Discussion		
5.1	Micro structural Characteristics	48
5.2	EDS Spectra	50
5.3	The Impedance Measurement	54
5.4	High Temperature Measurement	56
5.5	Magnetoresistance Measurement	57
5.6	Permeability Measurement	58
5.7	The Magnetization Measurement	61
5.8	DTA, TGA, DTG Analysis	64
5.9	Heat Diffusivity Measurement	67
Chapter Six : Conclusion and Future Work		
6.1	Conclusion	71
6.2	Suggestion for future work	72
List of symbols and nomenclature		73
References		75

Abstracts

The magnetic and structural properties of $(\text{Fe}_{100-x}\text{V}_x)_{75}\text{P}_{15}\text{C}_{10}$ alloys have been studied by measuring the magnetization and structural parameters. The samples are fabricated by conventional melt spinning technique at wheel speed of 25 m/sec. The as made samples are found to be ferromagnetic at room temperature and all of them go through the magnetic phase transition between 500 and 600 K. The magnetic phase transition of all the studied samples are observed to be around the glass transition temperature T_g which is between 650 to 700 K. The DTA and TGA data have shown some exothermic peaks above 700 K indicating some structural phase transformation above this temperature. All the studied samples have shown a small second peak at even higher temperature around 800 K which may be attributed to oxidation of the samples. Addition of Vanadium (V) has resulted in significant decrease in magnetization values. Addition of V is likely to have increase in grain size in a matrix of ferromagnetic Fe particles surrounded by the non-magnetic C and P atoms. However, an exceptional behavior was recorded for the sample $(\text{Fe}_{85}\text{V}_{15})_{75}\text{P}_{15}\text{C}_{10}$ which has shown a remarkable increase in magnetization values. The possible reason for this unusual behavior may be attributed to the formation of nano grains initiated by vanadium. This enhancement in magnetization has been supported by the magnetoresistance data which has also shown a remarkable increase in the magnetoresistance value for this particular concentration of V. The EDS analysis shows that addition of V did not cause any stoichiometric imbalance in the alloy system. Addition of V is expected to increase the coercivity of the alloy system and enhance the magnetic properties. However, from this study it is found that the role of V is similar to addition of a non-magnetic solute in a magnetic alloy which is depicted in the magnetization curves of all the studied samples. The impedance measurements on all the samples show a pronounced non linearity above 10 MHz with the exception of sample-3 in which contains 9 at% of V. Further detailed studies are needed to explain this behavior of the sample. The a.c. permeability studies show a systematic decrease in the a.c. magnetic response of the samples with increasing frequency.

Chapter One

Introduction



1.1 Introduction

Magnetic amorphous alloys obtained by rapid quenching of the melt are excellent soft magnetic materials with a wide range of technological applications. They also represent a significant challenge to the scientific understanding of magnetic materials, since most of the existing theories of solids assume lattice periodicity. For these reasons, the magnetic and other properties of amorphous alloys have been very actively studied over the last decade. In recent years, increasing attention has been directed to the fundamental understanding of the structural, thermal and magnetic properties of the amorphous alloys. It is not only scientifically but also technologically important to achieve such an understanding, since the amorphous alloys are, in many respects, so different from conventional crystalline magnetic materials.

A real technical interest developed after Pond and Maddin [1.1] reported on the preparation of continuous ribbons of amorphous alloy. Their method consisted essentially of directing a molten stream of the alloy onto the surface of a rapidly rotating drum. The present stages of work on amorphous ribbons originate from the study of Duwez et. al. [1.2] on the preparation and properties of amorphous alloys.

Theoretically expected retention of ferromagnetic behavior in amorphous solid was first demonstrated by Nowick et. al. [1.3] in their work on vacuum deposited Co-Au alloys and soon Tsuei and Duwez [1.4] on splat-cooled Pd-20 at % Si containing some ferromagnetic element partially substituted for the Pd. Simson and Brambly [1.5] appear to have been the first to point out that the amorphous alloys, expected to have no magnetocrystalline anisotropy, should have very low coercivities. However, the early amorphous alloys of CoP, prepared by deposition methods had coercivities as high as 10-20 (800-600) A/m. these high coercivities are now understood to have arisen from compositional inhomogeneties demonstrated by Chi and Cargill [1.6] from small angle X-ray scattering analysis and from strain-induced magnetostrictive anisotropy. The melt-quenched alloys of Fe-C appeared to be compositionally much more homogeneous but still developed coercivities of a few Oersteds (160 A/m), many orders of magnitude higher than in the Fe-Ni alloys. Amorphous alloys of Fe-Ni-P-B prepared by the melt-quenching technique as ribbons by solidification on the surface of a rapidly rotating drum exhibited even lower coercivities, in the order of 0.1 Oe (8 A/m).

Luborsky et. al. [1.7] first demonstrated the reduction of coercivity in these alloys, down to less than 10 mOe (90.8 A/m) by suitable annealing and showed that the changes in properties correlated to the relieving of internal strains. At that time Egami et. al. [1.8] showed that annealing under tensile stress reduced the coercivity of a Fe-Ni-p-B-Si alloy to 3 mOe (0.3 A/m).

There are two technologically important classes of magnetic amorphous alloys; the transition metal-metalloid (TM-M) alloys and the rare earth-transition metal (RE-TM) alloys. The TM-M alloys typically contain about 80 atom % Fe, Co, or Ni with the remainder being B, C, Si, P or Al as glass forming materials. The presence of the metalloids is necessary to lower the melting point, making it possible to quench the alloy through its glass temperature rapidly enough to form the amorphous phase. The present study involves the preparation of Fe based amorphous ribbons. In this amorphous ribbons P and C have been used as glass forming materials. Here the Fe have been partially replaced by V, the general composition being $(Fe_{100-x}V_x)_{75}P_{15}C_{10}$ [x=1.5, 3, 9, 15].

The melt-spinning technique has been used for the preparation of the ribbons. The methods of the preparation of the ribbons are described in Chapter-2 along with the procedure and conditions for glass forming amorphous materials.

The studies of the magnetic properties of amorphous ribbons are significant for a variety of applications such as power generator transformers, magnetic heads, magnetic shielding etc. These applications may be determined by static (dc) or dynamic (ac) properties of the amorphous system.

Moreover, the temperature dependence and the stability and cost of materials are to be considered besides their magnetic properties. The dc and ac properties provided characteristics suitable for different types of applications. Generally high electrical resistivity, high mechanical strength, good corrosion resistance, and absence of crystalline anisotropy, structural defects and grain boundaries characterize amorphous ribbons. The magnetic properties such as saturation flux density, Curie temperature, magnetostriction and induced anisotropy can be controlled by the alloy composition and a subsequent heat treatment.

The high electrical resistivity and the small thickness of the melt-quenched ribbons lead to low eddy current losses. The low hysteresis losses, results in very low core losses which is

of interest for power electronics at high frequencies. For application in small electronic devices, the amorphous ribbons have somewhat poorer losses and permeabilities than the conventional Fe-Ni-B ribbon. The design optimization requires lower cost of amorphous ribbons, higher induction compared to Fe-Ni-B ribbons. Amorphous ribbons have many refined applications also like development of magnetic bubbles for computer memory, amorphous superconductors etc. Research in the theoretical understanding, development and application of amorphous ribbons can thus be profitable, especially at its present new phase.

1.2 Aim of this Work

In recent years, amorphous alloys have received considerable experimental and theoretical attention owing to their anomalous magneto-transport and soft magnetic properties. These materials are interesting from both the fundamental and applied viewpoints. Because of various superior mechanical, magnetic and electrical properties, in comparison with those of the crystalline state, amorphous alloys form a class of technologically important materials. They have already been put into applications in the devices e.g., choke coils, high frequency transformers and the magnetic thin film heads, reported in 1991 by Yoshizawa *et al* [1.9].

The objective of this work is to study temperature and field dependence of electrical resistivity, magnetoresistance, frequency dependent complex permeability and impedance of $(\text{Fe}_{100-x}\text{V}_x)_{75}\text{P}_{15}\text{C}_{10}$ magnetic alloy, and effect of Vanadium (V) there on. The studies involved in the present work would provide useful information about its potentials in high frequency switching and sensor devices as well as high temperature power applications. In order to achieve the aforesaid objective, the following main steps are included in the present work:

1. The I-V measurement for resistivity and magnetoresistance in different magnetic fields at room temperature, high temperature and low temperature.
2. The measurement of ac permeability and impedance at different frequencies.
3. The measurement of heat diffusivity by an evacuated heat pulse for studying the information about the existence of a pseudo magnetic phase (antiferromagnetic/spin glass).

4. The measurement of magnetization in different magnetic field at room temperature to measurement the magnetic behavior of the samples.
5. The measurement of Thermal Analysis (DTA), Thermo Gravimetric Analysis (TGA, Differential Thermo Gravimetric (DTG) for the investigation of thermal response of the film.

Chapter Two

Preparation of Amorphous Ribbons

2.1 Introduction

Amorphous solid glass which has no precise meaning, it believed from the long time that amorphous system could not exist ferromagnetism. There are different methods produced to prepare the amorphous ribbons. This trend abolishes after the discovery of metallic glass by Dewez et. al. [2.1] and Gobonov [2.2] in the same time. There argument was based on the evidence that the electronic band structure of crystalline solids did not changes in any fundamental way on transition on the liquid state. The first report of an amorphous metallic alloy appears to have been made by Brenner et. al. [2.3]. A real technological interest developed after Pond and Maddin [2.4] reported on the preparation of continuous ribbons of amorphous alloys.

The technological interest developed after Pond and Maddin [2.4] reported on the preparation of continuous ribbons of amorphous alloys. The theoretically expected retention of ferromagnetic behavior in amorphous solids was first demonstrated by Marder and Nowick [2.5] in their work on vacuum deposited Co-Au alloys and soon there after by Tsuei and Duwez [2.6] in their work on split-cooled Pd-20at% Si containing some ferromagnetic element partially substituted for the Pd.

The positive way to have the amorphous state of pure metal like Fe, Ni, Co etc at low temperature. Alloys of these metals with glass forming materials can be obtained in the amorphous state by cooling the melt at a relatively lower rate of million degrees per second which can remain in the metastable state over an extended range of temperature.

Two important classes of amorphous magnetic materials are being studied intensively in recent time. They are the transition metal-metalloid (TM-M) glass and the rare-earth transition metal glass (RE-TM) reported by T. Mizoguchi [2.7], R. Alben et. al. [2.8] E. M. Gyorgy [2.9] and G. S. Cargil [2.10]. TM-M glasses are stable for composition around 75-80% of TM (Fe, Co, Ni etc. or in their combinations) and 25-20% of the metalloid (P, C, Si, B or in their combinations). Typical composition for RE-TM glass is RE₃₃-TM₆₇ where RE is one of the rare-earth metals like Gd, Tb, Dy, Y etc. and TM is one of the 3d transition metals like Fe, Co or Ni. Recently the metalloids in TM-M glass are replaced by non-magnetic metals like Zr, Hf, etc. by T. Masumoto *et. al* [2.11]. The new amorphous and metastable alloys prepared by such techniques were used in the early works to explore the many possibilities opened up by these new rapid quenching techniques.

2.2 Conditions to be prepared amorphous materials

In terms of viscosity and diffusion co-efficient we can find the conditions for formation glass.

- (a) Metals atomic bonding is metallic and viscosity is lower than the diffusion co-efficient and mobility is high.
- (b) In the case of amorphous material viscosity is very high and the mobility and the diffusion co-efficient are low. Atomic bonds tend to be covalent as in the case of silicate (SiO_2)

2.3 Preparation technique of amorphous ribbon

There are various techniques in use to produce a metallic alloy in an amorphous state where the atomic arrangements have no long-range periodicity. The different experimental techniques developed to produce amorphous metallic glass can be classified into two groups.

- (a) The atomic deposition methods and
- (b) The fast cooling of the melt

2.3.1 The atomic deposition methods

Deposition can be described in terms of whether the added atom is prevented from diffusing more than an atomic distance before it is fixed in position due to cooling and increased viscosity. The atomic deposition methods include condensation of a vapor on a cooled substrate by

- (i) Vacuum deposition
- (ii) Sputter deposition
- (iii) Electron deposition
- (iv) Chemical deposition

2.3.2 The fast cooling of the melt

For producing of an amorphous state by any of the liquid quenching devices, the alloy must be cooled through the temperature range from the melting temperature (T_m) to the glass transition temperature (T_g) very fast allowing no time for crystallization. The factors

controlling T_g and crystallization are both structural and kinetic. The structural factors are concerned with atomic arrangement, bonding and atomic size effects. The kinetic factors as discussed by Turnbull [2.12] are the nucleation, crystal growth rate and diffusion rate compared to the cooling rate. The interest in this method stems from the wide variety of alloys that can be made as well as from the potential low cost of preparation. In the pioneering work of Duwez et. al. [2.13], a number of devices has been reported for obtaining the necessary high quenching rates and for producing continuous filaments. The methods using the principle of fast cooling of melt techniques are:

- (i) The gun technique
- (ii) Single roller rapid quenching technique
- (iii) Double roller rapid quenching technique
- (iv) Centrifuge and rotary split quenching technique
- (v) Torsion catapult technique
- (vi) Plasma-jet spray technique
- (vii) Filamentary casting technique
- (viii) Melt extraction technique
- (ix) Free jet spinning technique and
- (x) The melt spinning technique

Although the different methods used in preparing amorphous metallic ribbons are mentioned here, only the melt spinning technique which was used to prepare the specimens for the present work will be discussed.

2.3.2.1 The Melt Spinning Technique

The metallic glasses are prepared by several methods employing special techniques which involve rapid solidification of the melt. Melt spinning is one such technique used to prepare metallic glasses. Certain alloys such as metal-metal ($\text{Cu}_{66}\text{Zr}_{33}$) and metal-metalloid alloys ($\text{Fe}_{80}\text{B}_{20}$, $\text{Pd}_{80}\text{Si}_{20}$) form glasses when they are quenched suddenly at an ultrafast cooling rate of 10^6 to 10^8 K per second. In order to prepare the above mentioned metallic glasses, the required quantity of metal-metal or metal-metalloid alloys are taken in a quartz tube in their stoichiometric ratio wt%. A set of heater coils surround the quartz tube at one end and the temperature of the heater coil is kept more than the melting point of the alloy compound. Therefore, the melt of the alloy compound

is formed at one end of the quartz tube. The melt is kept above the melting point of alloy until a homogeneous mixing is obtained. An inert gas is flown through the other end of the quartz tube after the homogeneous mixing is formed. The molten alloy flow through the outlet of the quartz tube and it is cooled at an ultrafast rate with the help of a rotating cooled copper cylinder. On impact with the rotation drum, the melt is frozen within a few millisecond producing a long ribbon of metallic glasses. The experimental set up used for the above process is shown in Fig- 2.1

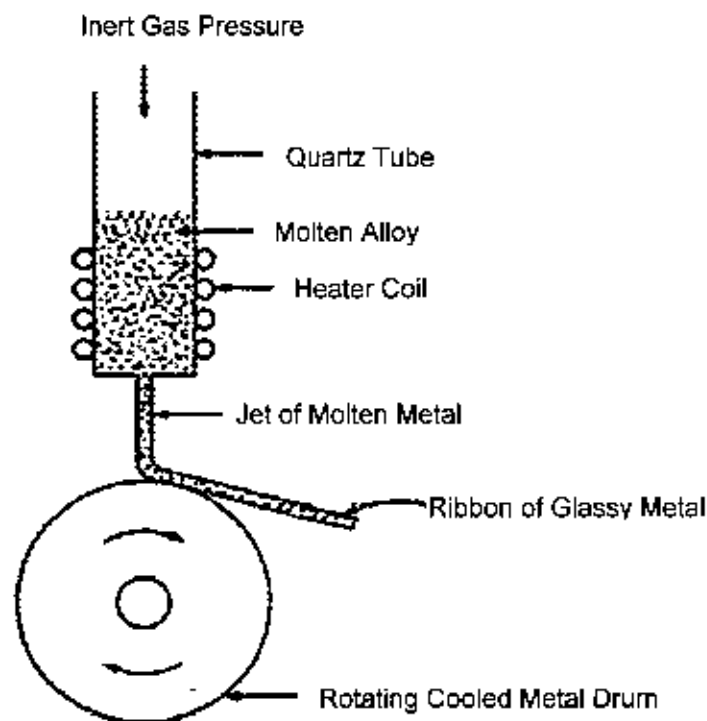


Figure 2.1: The experimental set up used for the melt spinning technique

2.4 Experimental details for the preparation of amorphous ribbon

The metallic glass ribbons are usually prepared in a furnace with an argon atmosphere (0.2 to 0.3 atms.). The buttons prepared are of about 50 grams each. Care is taken to ensure thorough mixing and homogeneity of the alloy composition, by turning over and re-melting each button few times. The mother alloys, formed in the form of buttons in a furnace by sudden cooling, are then cut into small pieces and is inserted in the quartz tube. The quartz tube is connected from the top by rubber 'O' rings and metal rings to the argon cylinder through a valve and a pressure gauge. After proper cleaning of the roller surface

and adjusting its speed to the desired value, as measured by stroboscope, the induction furnace is powered using high frequency generator. When the melting temperature is reached as observed through a protective spectacle, the injection pressure is applied by opening the pressure valve. To avoid the turbulence of the wind, arising from the high-speed roller in distributing the melt puddle, cotton pad and metallic shield are usually used just beneath the roller. To avoid oxidation of the ribbon during its formation, an inert atmosphere is created around the roller by a slow stream of helium gas. The speed of the roller, the volumetric flow rate, the orifice diameter, the substrate orifice distance, the injection angle etc. are adjusted by trial and error to get the best result in respect of the quality and the geometry of the ribbons. Important factors to control the thickness of ribbons are as follows

Rotating speed

- (b) Angular velocity, $\omega \sim 2000$ rev/min.
- (c) Surface velocity, $v \sim 20$ m/s
- (i) Gap between the nozzle and rotating copper drum is ~ 100 to $150 \mu\text{m}$.
- (ii) Oscillations of the rotating copper drum both static and dynamic have maximum displacement of $\sim 1.5 \mu\text{m}$
- (iii) Pressure = 0.2 to 0.3 argon atmosphere.
- (iv) Temperature of the metal $T_m \approx 1500^\circ\text{C}$. The temperature should not exceed 1800°C otherwise quartz tube would melt.
- (v) Stability is ensured for the drop to fall on the surface of the spinning drum.

2.5 Factors contributing to glass formation

There are three interrelated factors that determine glass-forming tendency. These are thermodynamic conditions that favor the liquid phase relative to the crystalline phase, the kinetic conditions that inhibit crystallization and the process factors that arise due to experimental conditions.

The thermodynamic factors for glass formation are liquids temperature T_m at which the alloy melts, the heat of vaporization and the free energy of all the phases that arise or could potentially arise during solidification process. Viscosity of the melt, the glass transition temperature T_g and the homogeneous nucleation rate belongs to kinetic parameters. The glass transition temperature is defined as the temperature at which the super cooled liquid takes on the rigidity of a solid of more specifically at which the viscosity approached 15 poise.

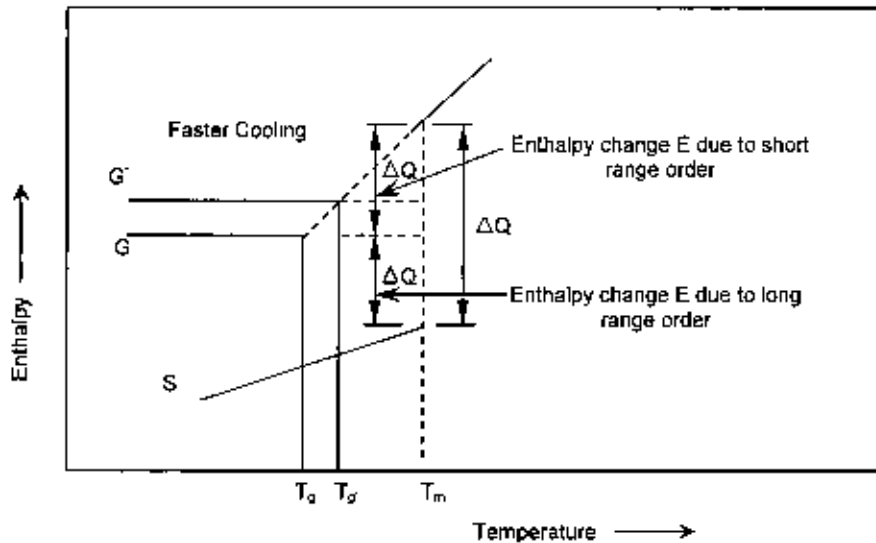


Fig 2.2: Temperature dependence of enthalpy H and G correspond to glass transition and S correspond to the crystalline state

Processing parameters are the cooling rate, the heterogeneous nucleation rate and the super cooling temperature interval. The temperature of the glass transition is slightly depend on the cooling rate at each cooling rate the glass will freeze in a different state of internal energy , shown in Fig 2.2.

At the melting point T_m the enthalpy H of a crystal includes latent heat of fusion due to long range order. In the case of rapid cooling of the melt, the free energy decreases since long range order do not take place, thus leaving the system at a higher energy rate. Heat treatment, relaxation and stability are thus important considerations in metallic glass. The glass-forming tendency also arises from as size difference between the components in the glassy alloy is a necessary condition for ready glass formation.

A single parameter that expresses glass forming tendency is the ratio of the glass transition temperature to the melting temperature defined as higher values of τ obviously favor glass formation. For metallic glass to be formed by rapid cooling, $\tau = \frac{T_g}{T_m}$ should be greater than

0.45 by H. S. Chem [2.14]. Based on alloy composition there are two major groups that rapidly form glasses. In one of these groups the metal is form Fe, Co, Pd, or Pt and the metalloid is B, C, Si, Ge, or P, these metallic glasses constitute soft amorphous magnetic materials.

Chapter Three

Theoretical Perspective

3.1 DC Electrical Resistivity

The law of electrical conduction in metals is obtained from Ohm's law which is given by

$$I = \frac{V}{R} \quad 3.1$$

Where, I is the current, V is the potential difference, and R is the resistance. From laws of resistance, we have

$$R = \rho \frac{L}{A} \quad 3.2$$

Where ρ is the resistivity that is the characteristic property of a metal, L is the length and A is the cross-sectional area of the material under test (MUT). Again by the definition of electric field, we know that the electric field, E is

$$E = \frac{V}{L} \quad 3.3$$

Now putting the values from equation- 3.2 and 3.3 into equation- 3.1, we get

$$I = \frac{EA}{\rho} \quad 3.4$$

In general the current density is defined, as the current per unit cross-sectional area of the specimen, hence, the current density using equation-3.4, will be as:

$$J = \frac{I}{A} = \frac{E}{\rho} = \sigma E \quad 3.5$$

Equation-3.5 is another form of Ohm's law, where σ is the electrical conductivity, which is again the inverse of resistivity ρ . Since the dimension of resistivity is ohm-m, so the conductivity σ has dimension (ohm-m)⁻¹.

Now we want to express σ in terms of the microscopic properties pertaining to the conduction electrons. These conduction electrons are responsible for the current flow under the influence of electric field because the ions are attached to and vibrate about their lattice sites. They have no net translation motion, and hence do not contribute to the current. For the purpose, let us now treat the motion of the conduction electron in an electric field. In this regard we consider one typical electron: The field exerts a force $-eE$ on the electron. There is also a frictional force due to collision of the form $-m^* \frac{v}{\tau}$, v is the velocity of the electron and τ is a constant called the collision time.

Using Newton's law of motion, we have

$$m^* \frac{dv}{dt} = -eE - m^* \frac{v}{\tau} \quad 3.6$$

Where m^* is the effective mass of electron. We see that the effect of the collision as usual in friction or viscous forces tends to reduce the velocity to zero. If we consider the steady-state condition for our purpose, then after putting $\frac{dv}{dt} = 0$, the appropriate solution of equation- 3.6 will be as:

$$v = -\frac{e\tau}{m^*} E \quad 3.7$$

This is the steady-state velocity of the electron, which is also known as terminal velocity that arises from the friction. It is opposite to the electric field, E because the charge of electron is negative. When a field is applied to a metallic wire/or material under test, there will be two different velocities associated with the electron. The velocity appearing in equation-3.7 is called the drift velocity. This is superimposed on a much higher velocity or speed, known as the random velocity that arises from the random motion of electron like gas even in the absence of electric field. This is due to the fact that the electrons move about and occasionally scatter and change direction. This random motion contributes zero current and also exists in the presence of electric field, but in that case, there is an additional net velocity opposite to the field, as given by equation- 3.7 v_d and v , denote these two velocities for distinction. Now the current density can be calculated from equation-3.7. Since there is a charge $(-Ne)$ per unit volume, and since each electron has a drift velocity given by equation-3.7, it follows that the amount of charge crossing per unit area per unit time is

$$J = -(Ne)v_d = -(Ne)\left(-\frac{e\tau}{m^*} E\right) = \frac{Ne^2\tau}{m^*} E \quad 3.8$$

This current is parallel to the electric field, E . Now comparing equation-3.5 and equation-3.8, we get the expression for the conductivity as:

$$\sigma = \frac{Ne^2\tau}{m^*} \quad 3.9$$

From equation-3.9, it is seen that σ increases as N increases. This is reasonable because N , the concentration, increases; there are more current carriers. The conductivity σ is inversely proportional to m^* which is also expected, since the larger m^* is, the more

sluggish the particle, and harder it is for move. The proportionality to τ follows because τ is actually the time between two consecutive collisions, i.e. the mean free lifetime. Therefore the larger τ is, the more time the electron has to be accelerated by the field between collisions. and hence the large the drift velocity (equation-3.7), and also the larger σ is. The time τ is also called the relaxation time. To see the reason for this naming, let us apply an electric field to the material long enough for a drift velocity $v_d(0)$ to be established. Now let the field is suddenly removed at some instant. The drift velocity after this instant is governed by the following relation with $E=0$ as:

$$m^* \frac{dv}{dt} = -eE - m^* \frac{v}{\tau}$$

$$\text{or } m^* \frac{dv}{dt} = - m^* \frac{v}{\tau} \quad 3.10$$

The solution appropriate to the initial condition is now

$$v_d(t) = v_d(0) e^{-\frac{t}{\tau}} \quad 3.11$$

Since t is the time between two successive collisions, it may be expressed as:

$$\tau = \frac{l}{v_r} \quad 3.12$$

Where l is the distance between two successive collisions and v_r is the random velocity. In terms of these σ becomes:

$$\sigma = \frac{Ne^2 l}{m^* v_r} \quad 3.13$$

Let us now discuss the origin of collision time. It seems natural to assume that the frictional force is caused by the collision of electrons with ions. According to this particular model of collision. an electron, as it moves in the lattice, collides with ions, which has the effect of slowing down the electrons momentum. This model turns out to be untenable because it leads to many points of disagreement with experiment. To cite only one: the mean free path l can be calculated from equation- 3.12. If we substitute the values $\tau \cong 10^{-14}$ s and $v_r = 10^6$ ms⁻¹, we find that $l = 10^2 \text{ \AA}$. This means that, between two collisions, the electron travels a distance of more than 20 times the inter-atomic distance, which one would expect. But in closed-packed structures, in which atoms are densely packed, it is difficult to see how the electrons could travel so far between collisions. This paradox can

only be explained by the use of quantum concept. According to quantum mechanics, an electron has a wave character. The De-Broglie relation gives this wavelength in the lattice:

$$\lambda = \frac{h}{m^* v_F} \quad 3.14$$

It is well known from the theory of wave propagation in discrete structures that, when a wave passes through a periodic lattice, it continues propagating indefinitely without scattering. The effect of atoms in the lattice is to absorb energy from the wave radiate it back, so that the net result is that the wave continues without modification in either direction or intensity. The velocity of propagation, however, is modified. This is what happens in the case of an electron wave in a regular lattice, except that in this case we are dealing with a matter wave.

3.1.1 Electrical Resistivity

In general, the resistivity is defined as the reciprocal of the conductivity, i.e.

$$\rho = \frac{1}{\sigma} = \sigma^{-1} \quad 3.15$$

Using equation- 2.9, we get the expression for the resistivity as:

$$\rho = \frac{m^*}{Ne^2} \times \frac{1}{\tau} \quad 3.16$$

We know from the interpretation that $\frac{1}{\tau}$ is actually equal to the probability of the electron suffering a scattering per unit time. Thus, if relaxation time is $\tau = 10^{-14}$ s, then the electron undergoes 10^{14} collisions in one second. But we saw that the electron undergoes a collision only because the lattice is not perfectly regular. We group the derivations from a perfect lattice into two classes

- a. Lattice vibrations (phonons) of the ions around their equilibrium position due to thermal excitation of the ions.
- b. All static imperfections, such as foreign impurities or crystal defects.

Among these the latter group we shall take impurities as an example. Now the probabilities of electrons being scattered by phonons and by impurities are additive, since these two mechanisms are assumed to act independently. Therefore, we may write

$$\frac{1}{\tau} = \frac{1}{\tau_{ph}} + \frac{1}{\tau_i} \quad 3.17$$

Where the first term on the right is due to phonons and the second term is due to impurities. The former is expected to depend on T and the later on impurities, but not on T. If we now substitute equation-3.7 into equation- 3.16, we readily find

$$\rho = \rho_i + \rho_{ph} = \frac{m^*}{Ne^2} \left(\frac{1}{\tau_{ph}} + \frac{1}{\tau_i} \right) \quad 3.18$$

From equation- 3.18 it is seen that has split into two terms: a term ρ_i is due to scattering by impurities, which is independent of temperature, called residual resistivity. Another term added to this is ρ_{ph} arises from the scattering by phonons and therefore temperature dependent. This is called ideal resistivity. Furthermore, since crystalline defects serve as scattering centers for conduction electrons in metals, increasing their numbers raises the resistivity. The concentration of these imperfections depends on temperature, composition, and the degree of cold work of a metal specimen. In fact, it has been observed experimentally that the total resistivity of a metal is the sum of the contributions of thermal vibrations, impurities and plastic deformation; that is, the scattering mechanism acts independently of one another. This may be represented in mathematical form as follows:

$$\rho = \rho_i + \rho_{ph} + \rho_d \text{ (plastic deformation causes by the magnetic annealing)} \quad 3.19$$

At low temperature, scattering by phonons is negligible because the amplitudes of oscillations are very small; in that region $\tau_{ph} \rightarrow \infty$, $\rho_{ph} \rightarrow 0$ and hence $\rho = \rho_i$ is a constant. As temperature increases, scattering by phonons becomes more effective and $\rho_{ph}(T)$ increases; this is why ρ increases. When temperature becomes sufficiently large, scattering by phonons dominates and $\rho \cong \rho_{ph}(T)$. In the high-temperature region, $\rho_{ph}(T)$ increases linearly with temperature. The part of ρ which is independent of temperature is called Matthiessen rule. From equation- 3.19, it is expected that ρ_i is proportional to the impurity concentration N_i . Resistivity linearly increases with temperature up to the melting point for the case of pure element.

3.2 Magnetoresistance

The magnetoresistance refers to the change in electrical resistance of a specimen in response to the magnetic field applied to the specimen externally. The resistance change occurs with the magnetic field when the field is sufficient enough to change the orientation

of the electrons of the atoms. In that case the path of the electron becomes curved and do not go exactly in the direction of the superimposed electric field. The change of orientation of the atomic electrons occurs such that the conduction electron find more mean free path with less number of collision with the atomic ions and the atomic electrons, then the resistance decreases other wise it increases or remain constant. When the resistance of a material changes with the application of the magnetic field then the material is said to have the magnetoresistance. The magnetoresistance usually expressed in percentage and is calculated by the following way

$$MR\% = \frac{R(B) - R(0)}{R(0)} \times 100\% \quad 3.20$$

Where, $R(B)$ is the resistance in presence of magnetic field and $R(0)$ is the resistance in absence of magnetic field.

All metals show some MR, but up to only a few percent. Nonmagnetic metals such as Au, exhibits small MR, but the magnitude is somewhat greater (up to 15%) in ferromagnetic metals such as Fe and Co. The semimetal Bi also shows ~18% MR in a transverse field of 0.6T which rises to a 40fold change at 24T [1]. Cu is more typical in the same very powerful field (24T) gives rise to change of only ~2% at room temperature. This is the classical positive magnetoresistance that varies as B^2 (B =applied magnetic field) in half metallic ferromagnets such as CrO_2 , Fe_3O_4 at low temperature [2]. It is absent in the free electron gas [3] but appears when the fermi surface is non spherical. This MR originates from the impact of the Lorentz force on the moving charge carriers similar to the Hall Effect. Its value is ~10% at 10T. A classification of magnetoresistance phenomenon is based on the distinction familiar in magnetism between intrinsic composition and purity and extrinsic properties of the sample.

The phenomenology of the magnetoresistance effect is similar to that of magnetostriction. This effect can be classified into two categories: one is the part, which depends on the intensity of spontaneous magnetization that corresponds to the volume magnetostriction. The second is that change caused by the rotation of spontaneous magnetization, which corresponds to the usual magnetostriction. Mort interpreted this phenomenon in terms of the scattering probability of the conduction electrons into 3d holes. If the substance is in a ferromagnetic state, half of the 3d shell is filled up, so that the scattering of 4s electrons into the plusd state of 3d shell is forbidden. This scattering is however, permitted in a nonmagnetic state in which both the plus spin state and the minus spin state of the upper

3d levels are vacant. Moti explained the temperature variation of resistivity fairly well by this model Kasuya interpreted this phenomenon from a standpoint quite different from Moti theory. He considered that d electrons are localized at the lattice points and interact with the conduction electrons through the exchange interaction. At 0^oK the potential for the conduction electron is periodic, because the spin of 3d electrons of all the lattice points point in the same direction. At finite temperature, spins of 3d electrons are thermally agitated and the thermal motion may break the periodicity of the potential. The 4s electrons are scattered by an irregularity of the periodic potential which results in additional resistivity. Kasuya postulated that the temperature dependence of the resistivity of ferromagnetic metal is composed of a monotonically increasing part due to lattice vibration and an anomalous part due to magnetic scattering, the magnitude of the later being explained by this theory. The effect of high temperature has been treated in two different approaches. The first approach is given by Harris *et. al.* [4] considers a constant exchange interaction between magnetic atoms and a random distribution of the local anisotropy field is considered which changes with temperature. The other approach is to consider a distribution of exchange integral is assumed in order to take into account the fluctuation in the amorphous alloys as taken by Handrich [5]. Both the approaches are unrealistic and in fact no rigorous theory of the high temperature behavior for amorphous material has been developed. We have determined the experimental power law from the temperature variation of magnetization in the high temperature range.

3.3 Impedance and the phases

Electrical impedance, or simply impedance, describes a measure of opposition to a sinusoidal alternating current (AC). Electrical impedance extends the concept of resistance to AC circuits, describing not only the relative amplitudes of the voltage and current, but also the relative phases. In general impedance is a complex quantity and the term *complex impedance* may be used interchangeably; the polar form conveniently captures both magnitude and phase characteristics,

$$\vec{Z} = Ze^{i\theta} \quad 3.21$$

where the magnitude gives the change in voltage amplitude for a given current amplitude, while the argument gives the phase difference between voltage and current. In Cartesian form,

$$\vec{Z} = R + iX \quad 3.22$$

where the real part of impedance is the resistance and the imaginary part is the reactance. Dimensionally, impedance is the same as resistance. And hence the impedance is regarded as the total resistance that a specimen shows. It is the total contribution from normal resistance, inductive reactance and capacitive reactance. The first one is frequency independent and the latter two are frequency dependent. The impedance is calculated as

$$Z = \sqrt{R^2 + X_C^2 + X_L^2} \quad 3.23$$

Where R is the normal resistance, X_C is the capacitive reactance and X_L is the inductive reactance. The term *impedance* was coined by Oliver Heaviside in July 1886. The SI unit is the ohm.

3.4 Inductive Reactance

Reactance is the imaginary part of impedance, a measure of opposition to a sinusoidal alternating current. Reactance arises from the presence of inductance and capacitance effect in the solid, and is denoted by the symbol, the SI unit is the ohm. When there is no capacitive effect the the reactance solely comes from inductance effect. With the application of a linear magnetic field to any substance, creates a circular current inside the substance. And that circular current provides a kind of resistance to the linear flow of further charges through the substance. This resistance is known as inductive reactance. The inductive reactance is calculated by

$$X_L = 2\pi fL \quad 3.24$$

Where f is the frequency and L is a constant known as inductance.

The Physical significance of the inductive reactance

Determining the voltage-current relationship requires knowledge of both the resistance and the reactance. The reactance on its own gives only limited physical information about an electrical component:

1. The value of the reactance is a lower limit on the magnitude of the impedance
2. A positive reactance implies that the phase of the voltage *leads* the phase of the current, while a negative reactance implies that the phase of the voltage *lags* the phase of the current

3. A reactance of zero implies the current and voltage are in phase (the only situation in which a specific value for the either the magnitude or phase of the impedance can be determined with knowledge of only the reactance) and conversely if the reactance is non-zero then there is a phase difference between the voltage and current

3.5 Inductance

When there is an arrangement of circulating current, a constant, called inductance, which exists between change in current and the flux linkage through the circulating current.

3.6 Permeability

Permeability is the degree of magnetization of a material that responds linearly to an applied magnetic field. Magnetic permeability is represented by the symbol μ . This term was coined in September, 1885 by Oliver Heaviside.

In SI units, permeability is measured in henrys per metre, or newtons per ampere squared. The constant value μ_0 is known as the magnetic constant or the permeability of vacuum. The permeability can be given as

$$\mu = \frac{\vec{B}}{H} \quad 3.25$$

Where, B is the magnetic flux density produced by the magnetizing force H.

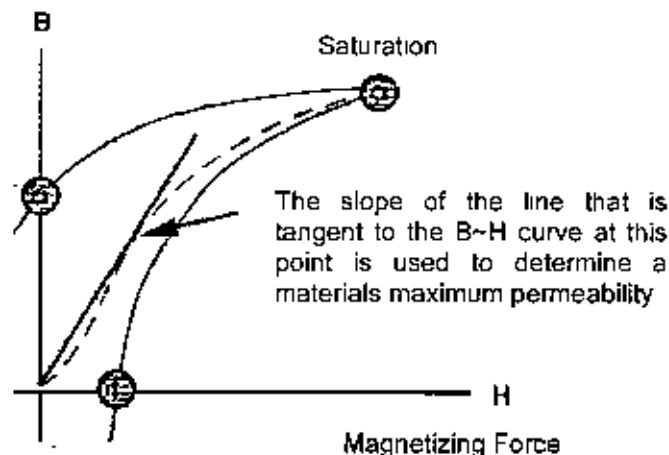


Figure-3.1: B~H Curve illustrates the procedure to determine the permeability

It is clear that this equation above describes the slope of the curve at any point on the hysteresis loop. The maximum permeability is the point where the slope of the B-H curve for un-magnetized material is the greatest. This point is often taken as the point where a straight line from the origin is tangent to the B/H curve. The relative permeability is defined as the ratio of the material's permeability to the permeability in free space.

$$\mu_r = \frac{\mu}{\mu_0} \quad 3.26$$

Where, $\mu_0 = 4\pi \times 10^{-7} \text{ H/m}$

The measurement of permeability has significant role to detect hard magnetic materials as well as soft magnetic materials. For hard magnetic materials, the value of the relative permeability is low that in turn leads to have high coercive field. On the other hand, the high permeability is the indication of soft magnetic materials that in turn leads to have low coercive field.

The above discussion on permeability is only considering the application of static fields. The dynamic response of the magnetic domains to the external field determines the complex permeability. The value of complex permeability provides the information about the inertia of the domains, their distribution and mutual coupling. The phase lag between the applied field and the response of magnetic domains determine the real μ' and imaginary μ'' parts of the complex permeability.

As the desirable properties for soft magnetic materials are high permeability and low loss so we have to consider the losses and resonance, which affect the permeability of soft magnetic materials in various ranges of frequencies. If a magnetic material is magnetized by the alternating magnetic field, $H = H_0 e^{j\omega t}$, that magnetic flux density of B is generally delayed by the phase angle δ because of the presence of loss and is thus expressed as $B = B_0 e^{j(\omega t - \delta)}$. The permeability is then will be a complex one and can be expressed as:

$$\mu = \frac{B}{H} = \frac{B_0 e^{j(\omega t - \delta)}}{H_0 e^{j\omega t}} = \frac{B_0}{H_0} e^{-j\delta} = \mu' - j\mu'' \quad 3.27$$

where, μ' is the real part which is actually the energy storage part and μ'' is the imaginary part which is called loss factor. This complex permeability is then related to two different

magnetizing mechanisms. One is the spin rotational magnetization and the other is the domain wall motion. In order to explain, we can consider the hysteresis loop, which is the magnetization trace owing to the alternating magnetic field, applied to the sample. This hysteresis implies the existence of energy losses in the system and these losses are proportional to the area of the loop.

3.7 Heat Diffusivity

The rate at which the material bar gets heated in the transient heat transfer problem before reaching of the steady state depends not only on the thermal conductivity but also on the thermal capacity and consequently is different for different materials. The rate at which the temperature of any part of the bar changes is determined by a quantity which has been called heat diffusivity or thermal diffusivity by Lord Kelvin and thermometric conductivity by Maxwell. If s denotes the specific heat and ρ the density (mass per unit volume) of the material of the bar, then the heat diffusivity (D) of the bar is given by

$$D = \frac{\text{Thermal Conductivity}}{\text{Thermal Capacity per unit volume}}$$

$$\text{i.e. } D = \frac{K}{\rho s} \quad 3.28$$

The diffusivity is a measure of how quickly a body can change its temperature, it increases with the ability of a body to conduct heat and it increases with the amount of heat needed to change the temperature of a body (s). The higher the thermal diffusivity, the faster the heat propagation. It has the dimension length²/time and has units of cm² s⁻¹. For common rock material, $K = 10^{-2}$ cm²s⁻¹. A high thermal diffusivity inhibits convection. All the three quantities on the right hand side of equation 3.28 as well as the thermal diffusivity can be function of temperature.

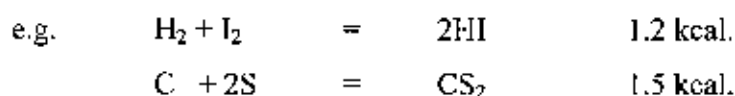
3.8 Differential Thermal Analysis (DTA)

DTA means the differential thermal analysis. Differential thermal analysis is the process of accurately measuring the difference of temperature in between the test sample and the reference when both are being heated or cooled at the same rate under, identical environment. Differences in temperature between the test sample and reference may arise,

when physical or chemical changes take place in the test material. The change of temperatures are observed either by endothermic or exothermic peak as a function of time or temperature. These changes may due to dehydration, transition from one crystalline variety to another, destruction of crystalline lattice, oxidation, hydrogenation, melting and boiling of the materials etc. Hence reference is used as a baseline which is thermally stable and unreactive i.e. no reaction can take place with in the ref. sample.

3.8.1 The endothermic and exothermic reactions

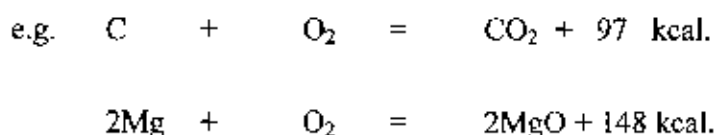
Reactions are accompanied by the absorption of heat is known as endothermic process or reactions. Reactions of this type require a continuous supply of energy from the outside to keep them going. For example, the decomposition of potassium chlorate into potassium chloride and oxygen will take place only so long as the compound is heated from outside. Similarly, the reaction of hydrogen and iodine to form hydro-iodic acid takes place with absorption of heat.



The compounds which are formed by endothermic reactions, such hydrogen peroxide, H_2O_2 and hydro-iodic acid, HI, are thermally unstable. This means that the internal energies of the molecules of H_2O_2 and HI tend to break the bonds holding the atoms together.

3.8.2 Exothermic reaction

The reactions which are accompanied by the evolution of heat, is known as the exothermic reaction. Exothermic reaction may proceed in the absence of any supply of energy from outside. The burning of magnesium, carbon, methane, etc, in air, are all exothermic reactions.



Thus, carbon will continue to burn in oxygen with the evolution of heat until the supply of carbon or oxygen is exhausted. It may be noted here that compounds which are formed by



highly exothermic reactions, such as carbon dioxide, magnesium oxide, are stable towards heat. These are said to be thermally stable. This means that a very high temperature is required to separate them into their component elements.

3.8.3 Peak Area, Peak Temperature, Effect of heating rate

When no reaction occurs in the specimen then no temperature difference between the specimen and the reference sample is observed but as soon as a reaction commences the specimen becomes hotter or cooler than the inert material and a peak develops on the curve for temperature difference against time ($\Delta T/t$) or temperature ($\Delta T/T$).

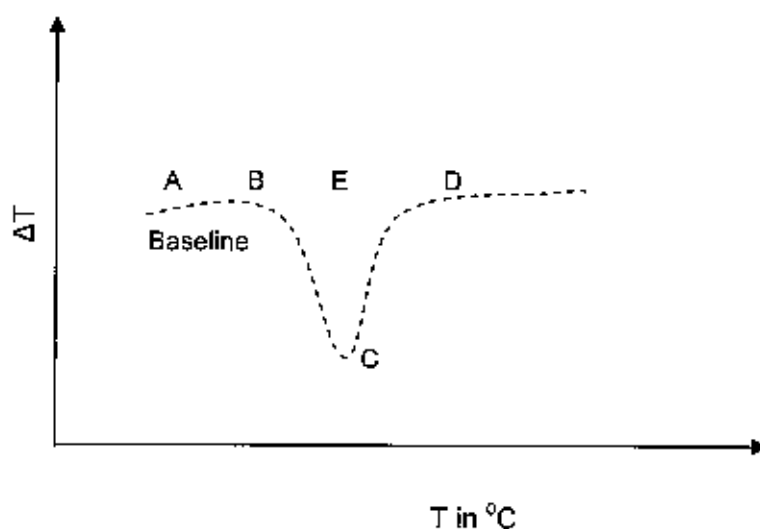


Figure 3.2. The DTA Curve explanation

Along the line AB the difference is zero since no reaction is occurring but at B an endothermic reaction starts and gives rise to the peak BCD with its minimum at C, where, the rate of heat absorption by the reaction is equal to the difference between the rate of supply of heat to the specimen and to the inert material.

Peak area ($BC \times DE$) is proportional to the amount of reacting material. The distance BD is usually referred as the peak width and the distance EC as the peak height or amplitude.

The area enclosed by the peak has to be accurately determined for quantitative work. In this method two tangents are drawn on both sides of the peak and a straight line AB joined the points of tangency. The area enclosed by ABC formed the peak area.

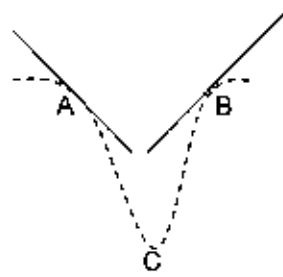


Figure 3.3: DTA peak analysis

3.8.4 Peak area function

It is convenient to introduce a function,

$$W(p) = \int_{t_0}^{t_1} \{T - T(p, t)\} dt$$

Where at the quasi-steady state (i.e. no reaction begins in the time $t < t_0$ to the assembly which attains a quasi-steady state), the temperature is given by

$$T = \beta t - fp$$

And t_2 is a time sufficiently long after the completion of the reaction for the system to have returned to the quasi-steady state. We shall call W the peak area function.

$$W(p) = \int_{t_0}^{t_2} \{\beta t - f(p) - T(p, t)\} dt$$

If areas below the base line are regarded as positive and those above negative, the peak area is

$$\begin{aligned} & \int \{(\Delta T)_0 - (\Delta T)\} dt \\ &= \int_{t_0}^{t_2} \{-f(p_1) + f(p_2) - T(p_1, t) + T(p_2, t)\} dt \\ & \text{by } (\Delta T)_0 = T(p_1) - T(p_2) \\ & \quad = -f(p_1) + f(p_2) \\ &= \int_{t_0}^{t_2} \{\beta t - f(p_1) - T(p_1, t)\} dt - \int_{t_0}^{t_2} \{\beta t - f(p_2) - T(p_2, t)\} dt \\ &= W(p_1) - W(p_2) \end{aligned}$$

The peak area $W(P_1) - W(P_2)$ is proportional to the heat of reaction per unit volume of the test sample.

The peak area is thus independent of (a) the heating rate, provided that it is linear; (b) the rate at which the reaction takes place; (c) the specific heat of the test sample. It does, however, depend on the conductivities of the test sample and of the other materials in the furnace and on the conductance between the surface of the block and the furnace wall.

3.8.5 Effect of heating rate

Peak area increases with rapid change of temperature (i.e. rate of heating). Peak shape changes with finer particle size to more reaction centers. The random stacking of the layers, coupled with disruption caused by removal of inter layer water, would be expected to expose more nuclei to dehydration at any moment for a given weight of mineral as slow heating rate reduces the sharpness of the peaks unduly and very fast rates tend to cause overlapping of neighboring reactions.

3.8.6 Transition state

A chemical reaction is presumably a continuous process involving a gradual transition from reactants to produce an arrangement of atoms at an intermediate stage of reaction as though it is an actual molecule. This intermediate structure is called the transition state. The reaction sequences are as follows.



ΔH is the difference in energy content between reactants and products, so E_{act} is the difference in energy content between reactant and transition state.

3.8.7 Activation Energy E_{act}

The minimum amount of energy that must be provided by a collision for reaction to occur is called the activation energy. It is denoted by E_{act} . When heat is liberated, the heat content enthalpy H of the molecules themselves must decrease, the change in heat content. Δh is therefore given a negative sign. (In the case of an endothermic reaction, where heat is absorbed, the increase in heat content of the molecules is indicated by a positive ΔH)

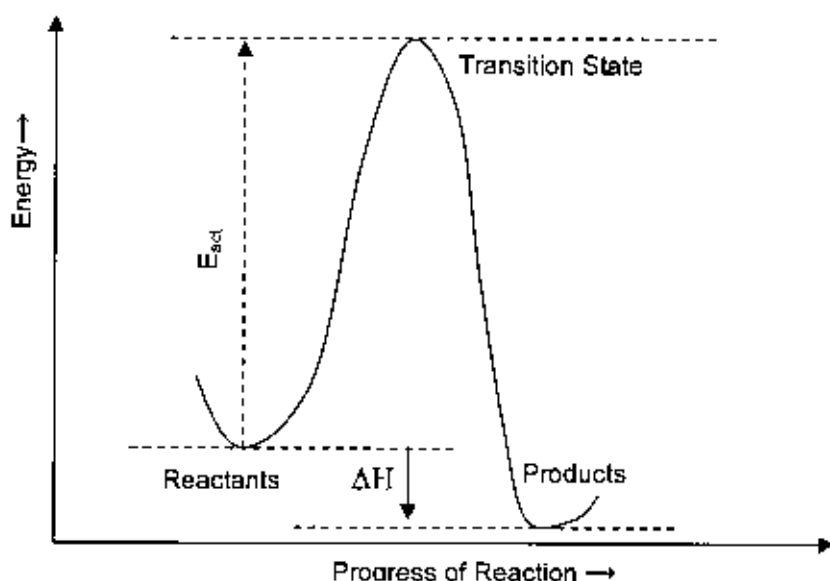


Figure 3.4: Activation energy for a reaction to start in DTA experiment

3.8.8 Change of Phase

A change of phase or phase change occurs when a crystalline solid becomes liquid or when a liquid becomes a vapor, or when the reverse of either of these processes takes place.

3.8.9 The latent heat in phase changes

During a change of phase, heat is either absorbed or given out by the material undergoing the change without any alternation in the temperature. We thus define the latent heat of fusion as the amount of heat required to convert unit mass of solid into liquid at the transition temperature (the same amount of heat is given out in the reversion process). The latent heat of vaporization is the amount of heat required to convert unit mass of liquid into vapor at the transition temperature and the same amount is given out when the vapor condenses.

3.8.10 Entropy and Disorder

Entropy may be defined in terms of the degree of disorder or randomness of a system. Solid crystalline has the regularity and symmetry of the distribution of the atoms which are arranged in an ordered way over large distances. They are said to have "long range" order.

It can be seen that at each phase change there is an increase in the randomness of the atoms and a corresponding increases in the entropy, when heat is supplied at such a temperature that a phase change does not take place ($T \neq T_B$ or T_m).

The increase in entropy is associated with the increase in temperature of the substance. This again represents an increase in the randomness of the atoms, which are then subject to greater thermal agitation. In general an increase in entropy is associated with an increase in disorder.

From a thermodynamic point of view, the effect of pressure is often competitive with that of temperature. In general, an increase in temperature tends to melt a solid and produce a less ordered system, while an increase in pressure tends to maintain an ordered phase. This creates the possibility that an isotropic liquid phase of carbonizing system may be favorably transformed, under pressure, into an optically anisotropic liquid crystal.

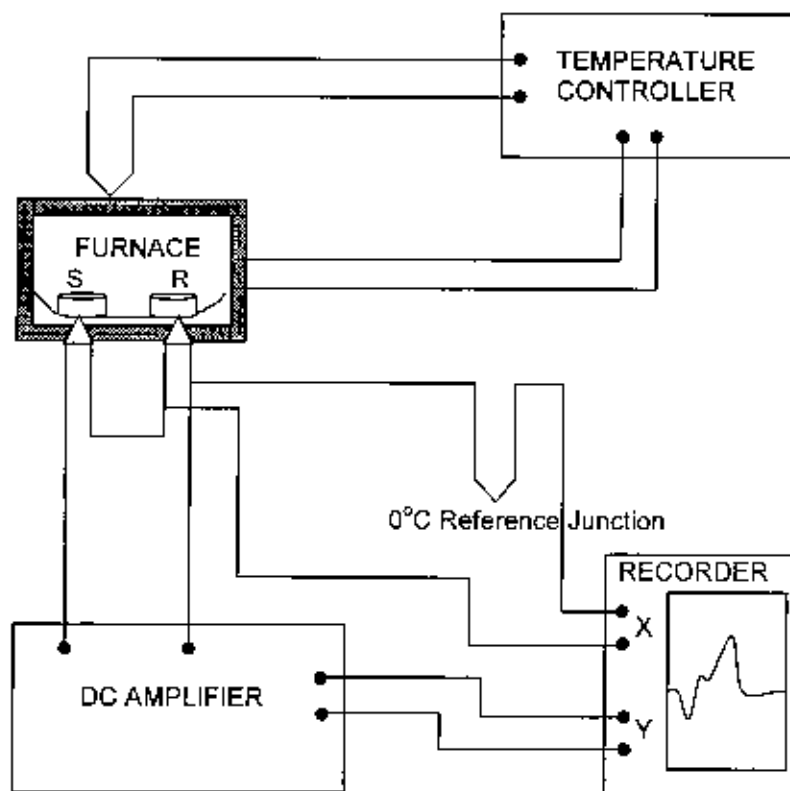


Figure 3.5: A Schematic diagram of the DTA assembly.

3.8.11 Experimental set-up of the DTA apparatus

- DTA assembly consists of a sample holder to place the sample.
- Thermocouples for measuring temperatures.
- A furnace to heat the sample
- A program controller to heat the sample at a uniform rate.
- And a recorder for registering the temperature difference between the sample and the reference material.

3.8.11.1 Sample Holder

Sample holder may be different size and shape and made of different materials. The most important prerequisite is that the sample holder should not itself undergo any thermal transformation and should not interact with the sample.

Usually the sample holder contains two cavities, one for housing the sample and the other for the reference material. Several materials have been used to make the sample holder. These materials may be, sintered alumina, fused quartz, Vycor glass, Porcelain, Silica, Zirconia, beryllia, graphite, Pyrophyllite, Nickel, Platinum, Crucible, Silver, Aluminum, inconel, Stainless Steel, depending on the temperature range.

3.8.11.2 Thermocouples

Thermocouple is used as a temperature measuring device. It measures the differential temperature as well as the temperature of the reference material or of the furnace. The emf of the thermo couple should be almost linear with respect to the changing temperature. Depending on the diff-temperature ranges there are various types of thermo couple used.

- A chromel-alumel thermo couple upto 1200°C
- A Copper-constantan thermo couple from -185 to 370°C
- Platinum-platinum + 10% Rhodium upto 1480°C
- Tungsten-molybdenum upto 2200°C
- Tungsten-graphite upto 2400°C
- Tungsten-tungsten + 26% rhenium upto 2850°C
- A graphite-tantalum carbide upto 3000°C

Thermo couples are connected in series form and what is known as a thermopile this method may be used to increase the electromotive force of a thermo couple.



The accuracy of the DTA interpretation is very much dependent on the measuring temperature. The quantitative DTA requires calibration with substances that have known the latent heats of fusion. Various substances have been suggested for calibration.

3.8.11.3 Furnace

Furnaces are either of vertical or horizontal type. They are usually tubular and heated by resistance elements. Various types of heating elements are used for temperatures up to 2800°C

3.8.11.4 Temperature Controller

A temperature controller is used just to control the temperature of the furnace. In an automatic method the voltage input to the heating element is controlled by a variable transformer through a synchronous motor.

3.8.11.5 Recorder

Various types of recorder are used for registering the differential temperature. In the earlier studies the differential temperature was recorded by a sensitive galvanometer or was automatically recorded on a photographic paper attached to a rotating drum. Pointer of sensitive galvanometer & photographic drum are rotating perpendicular to each other. Most of the commercial recorders available to day use electronic potentiometric recorders that simultaneously record the differential as well as the temperature of the reference material.

- A DC Amplifier is used to amplify the differential signal before feeding to the recorder.

3.9 Thermo Gravimetric Analysis (TGA)

The thermo Gravimetric analysis (TGA) are often called TG% and been done with the experiment of DTA at the same time to compare the result of DTA and TG% to find out more accurately what happened in the test material at each rising temperatures. The TG% means the mass loss or mass gain at different temperatures often calculated at percentages. The TG% results are usually shown in graphical mood in which the temperature or time is plotted against mass change in percentage. When any reaction occurs, the reaction may be endothermic or exothermic

may also associated with mass change due to evaporation of fundamental element from the sample or may be the mass gain due to new formation of compound. The TG% peak helps to analyze the DTA curves more accurately.

3.10 Differential Thermo Gravimetric (DTG)

DTG calculates the rate of mass change at any temperature with respect to the differential change of temperature or time at that temperature. This calculation is done in association with a TG% analysis. It is done for the following reason. Some time in TG% curve, there may be one peak due to two or more successive reactions that happens with in a very short time interval and that cannot be detected with the TG peak. TG% gives one peak for very close successive reactions. On the other hand the DTG peaks are so useful tool that it can differentiate very clearly that closed reactions with giving separate peaks for each of the successive reactions.

In DTG analysis the $\frac{dm}{dT}$ is plotted against Temperature T or time t in the other axis. At the peak the rate of mass loss/gain is maximum. The area under the DTG peak is proportional to the mass change dm . Height of the peak at any time or temperature indicates the rate of mass change at that temperature.

3.11 Scanning Electron Microscopy

Electron microscopy takes advantage of the wave nature of rapidly moving electrons. Where visible light has wavelengths from 4,000 to 7,000 Angstroms, electrons accelerated to 10,000 keV have a wavelength of 0.12 Angstroms. Optical microscopes have their resolution limited by the diffraction of light to about 1000 diameters magnification Electron microscopes, so far, are limited to magnifications of around 1,000,000 diameters, primarily because of spherical and chromatic aberrations. Scanning electron microscope resolutions are currently limited to around 25 Angstroms, though, for a variety of reasons.

The scanning electron microscope generates a beam of electrons in a vacuum. That beam is collimated by electromagnetic condenser lenses, focused by an objective lens, and scanned across the surface of the sample by electromagnetic deflection coils. The primary imaging method is by collecting secondary electrons that are released by the sample. The secondary electrons are detected by a scintillation material that produces

flashes of light from the electrons. The light flashes are then detected and amplified by a photomultiplier tube.

By correlating the sample scan position with the resulting signal, an image can be formed that is strikingly similar to what would be seen through an optical microscope. The illumination and shadowing show a quite natural looking surface topography.

There are other imaging modes available in the SEM. Specimen current imaging using the intensity of the electrical current induced in the specimen by the illuminating electron beam to produce an image. It can often be used to show subsurface defects. Backscatter imaging uses high energy electrons that emerge nearly 180 degrees from the illuminating beam direction. The backscatter electron yield is a function of the average atomic number of each point on the sample, and thus can give compositional information.

Scanning electron microscopes are often coupled with x-ray analyses. The energetic electron beam - sample interactions generate x-rays that are characteristic of the elements present in the sample. Many other imaging modes are available that provides specialized information.

3.11.1 Working Function of SEM

The "Virtual Source" at the top represents the electron gun, producing a stream of monochromatic electrons.

- (a) The stream is condensed by the first condenser lens. This lens is used to both form the beam and limit the amount of current in the beam. It works in conjunction with the condenser aperture to eliminate the high-angle electrons from the beam
- (b) The beam is then constricted by the condenser aperture, eliminating some high-angle electrons
- (c) The second condenser lens forms the electrons into a thin, tight, coherent beam and is usually controlled by the "fine probe current knob"
- (d) A user selectable objective aperture further eliminates high-angle electrons from the beam
- (e) A set of coils then "scan" or "sweep" the beam in a grid fashion (like a television), dwelling on points for a period of time determined by the scan speed (usually in the microsecond range)

- (f) The final lens, the objective, focuses the scanning beam onto the part of the specimen desired.
- (g) When the beam strikes the sample (and dwells for a few microseconds) interactions occur inside the sample and are detected with various instruments
- (h) Before the beam moves to its next dwell point these instruments count the number of interactions and display a pixel on a CRT whose intensity is determined by this number (the more reactions the brighter the pixel).
- (i) This process is repeated until the grid scan is finished and then repeated. the entire pattern can be scanned 30 times per second.

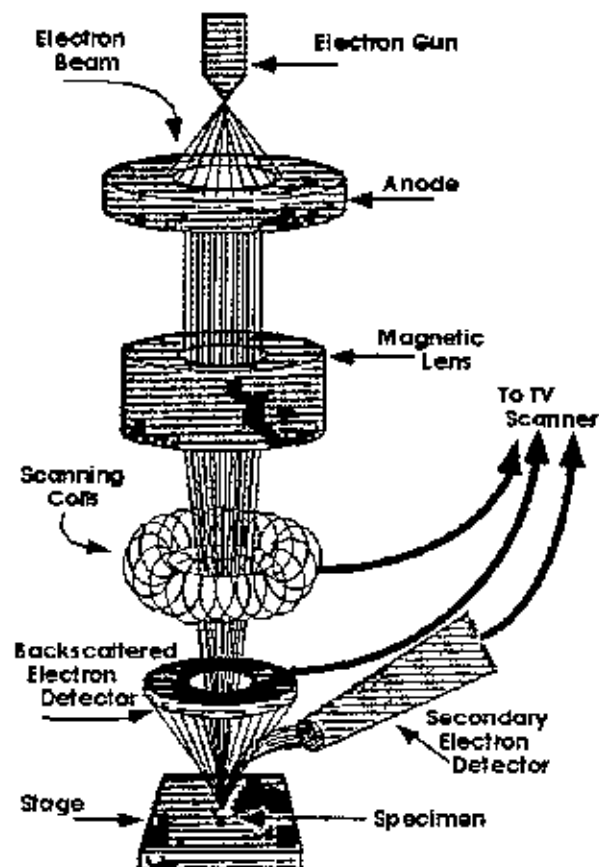


Fig -3.6: Schematic diagram of an SEM

SEMs are patterned after Reflecting Light Microscopes and yield similar information

3.11.2 Topography

The surface features of an object or "how it looks", its texture; detectable features limited to a few nanometers

3.11.3 Morphology

The shape, size and arrangement of the particles making up the object that are lying on the surface of the sample or have been exposed by grinding or chemical etching; detectable features limited to a few nanometers

3.11.4 Composition

The elements and compounds the sample is composed of and their relative ratios, in areas - 1 micrometer in diameter

3.11.5 Crystallographic Information

The arrangement of atoms in the specimen and their degree of order; only useful on single crystal particles >20 micrometers.

3.12 Working Principle of Vibrating Sample Magnetometer (VSM)

The vibrating sample magnetometer has become a widely used instrument for determining magnetic properties of a large variety of materials: diamagnetic, paramagnetic, ferromagnetic and antiferromagnetic. It has a flexible design and combines high sensitivity with easy of sample mounting and exchange. Samples may be interchange rapidly even at any operating temperature. Measurements of magnetic moments as small as 5×10^{-5} emu are possible in magnetic fields from zero to 4 Tesla. Maximum applied fields of 2-3 Tesla are reached using conventional laboratory electromagnets. Vibrating sample magnetometers normally operate over a temperature range of 20 to 1050 K.

Principle:

If a sample of any material is placed in a uniform magnetic field, created between the poles of an electromagnet, a dipole moment will be induced. If the sample vibrates with sinusoidal motion a sinusoidal electrical signal can be induced in suitable placed pick-up coils. The signal has the same frequency of vibration and its amplitude will be

proportional to the magnetic moment, amplitude, and relative position with respect to the pick-up coils system.

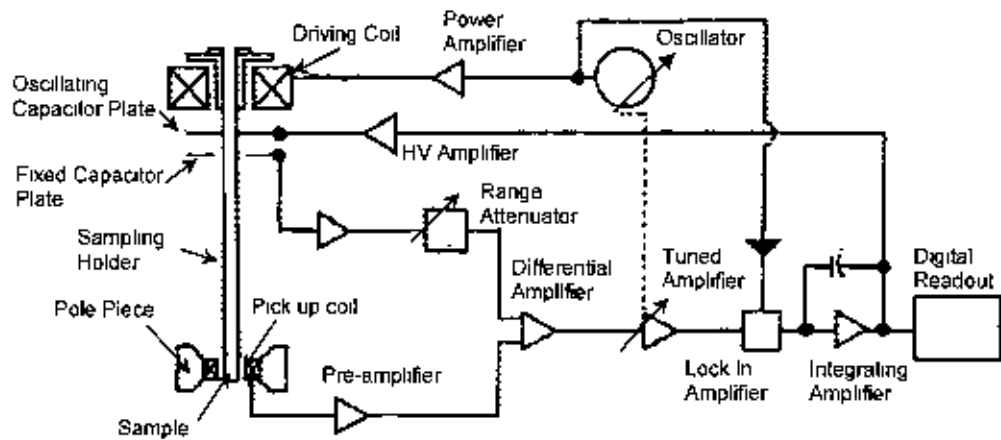


Fig. 3.7 Block diagram of Vibrating Sample Magnetometer.

The sample is fixed to a small sample holder located at the end of a sample rod mounted in a electromechanical transducer. The transducer is driven by a power amplifier which itself is driven by an oscillator at a frequency of 90 Hertz. So, the sample vibrates along the Z axis perpendicular to the magnetizing field. The latter induced a signal in the pick-up coil system that is fed to a differential amplifier. The output of the differential amplifier is subsequently fed into a tuned amplifier and an internal lock-in amplifier that receives a reference signal supplied by the oscillator. The output of this lock-in amplifier, or the output of the magnetometer itself, is a DC signal proportional to the magnetic moment of the sample being studied. The electromechanical transducer can move along X, Y and Z directions in order to find the saddle point (which Calibration of the vibrating sample magnetometer is done by measuring the signal of a pure Ni standard of known the saturation magnetic moment placed in the saddle point.

Chapter Four

Experimental Techniques

4.1 Techniques for DC electrical measurement with magnetic field

There are various types of electrical methods for resistivity/conductivity measurements. Out of these, 2-probe and 4-probe methods are widely used in measurements.

4.1.1 DC electrical resistivity: 2- probe and 4-probe method

The electrical conductivity is a technologically important parameter. There are two simple types of specimen and electrode arrangements that are basic to volume resistivity measurements:

- One is a rectangular or cylindrical block with electrodes on the ends.
- The other is like that used for dielectric measurements where electrodes are applied to either side of a thin disk.

The later is more appropriate for high resistivity measurement. In both cases, the volume resistivity is related to the measured resistance R between the electrodes by

$$\rho = \frac{RA}{L} \quad 4.1$$

where A and L are the cross-sectional area and the length or thickness of the specimen between the electrodes respectively. A main problem is that of contact resistance. Somehow we must connect electrodes between the sample and the external circuit and this involves the making "contact" to the sample. Contacts are notorious sources of, resistance (and noise). Moreover, as the contact involves an interface between two dissimilar materials, its I-V characteristics are frequently nonlinear, i.e., it may not be ohmic. Any effect of contact resistance should be avoided; provided that the contact resistance is much smaller than that of input resistance of the voltmeter. For accurate measurement the contact resistance may also reduced by pointing electrodes directly onto the surface of the specimen instead of relaying on pressure contact with metal plates or foils. Suitable point, are silver dispersion or aquadag (an aqueous dispersion of colloidal graphite).

For the measurements of high resistivity, the main problem is the leakage of current and one can overcome this problem to a large extent by the use of an extra guard electrode on the specimen. The standard way to separate out the sample resistance from the contact resistance is to use a 4-terminal potentiometric methods as in Fig-4.1. By separating the current contacts from the voltage contacts we are able to distinguish the sample resistance

from that of the contacts and connecting electrodes. Let a uniform current density j is established throughout the conductor by a battery connected to the outer electrodes. If the electric field E is determined by measuring the potential drops ΔV across two inner electrodes separation the resistivity is given by

$$\rho_v = \frac{j}{E} = \frac{\frac{j}{A}}{\frac{\Delta V}{\Delta x}} \quad 4.2$$

Now, if the conductor is not of uniform cross-sectional area, but instead, had some narrow regions and some wider regions, this expression no longer holds. In general, the measured resistance is some weighted average of the resistivity over the volume of the conductor.

The "weighting" is determined by the square of the current density, $\vec{j} \cdot \vec{j}$

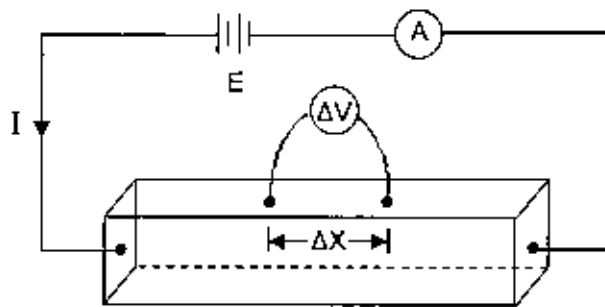


Fig 4.1: Circuit showing a four-probe resistance measurement.

When current enters a conductor through a point contact, the current density in the sample immediately under the contact is very large [1]. "Downstream" the current quickly spreads and at the exit contact, the current again must "Crowd" into the point contact. The "effective" sample resistance (even if it did not include electrode and contact interface resistances) it is not simply $\rho(L/A)$, due to the non-uniform current density. Even if we are willing to integrate the weighting function, it is critically sensitive to the exact contact area, which is hard to determine.

The problem is avoided with a four-probe measurement like that Fig. 4.1. The situation at the current contacts has not improved. The improvement comes in that we measure the voltage drop "downstream" where the current density has become uniform. Now the

resistance may be used to calculate the sample resistivity using the separation distance of the voltage probes for L .

There is one other important kind of four-probe resistivity measurement that we will find useful. This involves setting four equally spaced point contacts down on the surface of a "large" conductor, as shown in Fig. 4.2. Let 'a' be the probe spacing and 'h' be the sample thickness. We assume that the sample is infinite (i.e., its horizontal dimensions are much larger than the probe spacing). A known current I is injected through the sample via the outer two probes, and the voltage drop ΔV is measured between the inner two probes. We may consider two cases:

- (i) the sample is infinitely thick (i.e., $h \gg a$), and
- (ii) the sample is infinitely thin (i.e., $h \ll a$),

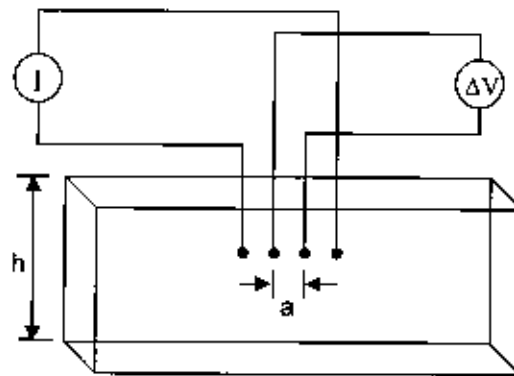


Fig 4.2: Four-probe method for measuring sheet resistance

Now let us try to visualize the current-density lines for this situation. Lines of \vec{j} look much like the electric field lines for a dipole in 3-dimensions for case 1, and 2 dimensions for case 2. Current enters the sample at the current contacts and quickly spreads. Underneath the voltage contacts, the lines of \vec{j} are determined, not by the nature of the contacts, but by the dimensionality of the conductor. For these two cases, the appropriate integrals have been performed to give the sample resistivity in terms of I and ΔV .

The results are:

$$h \ll a: \quad \rho = \frac{\pi h}{\ln(2)} \left(\frac{\Delta V}{I} \right) \quad 4.3$$

$$h \gg a: \quad \rho = 2\pi a \left(\frac{\Delta V}{I} \right) \quad 4.4$$

For the two dimensional case, the quantity ρ/h (which has units of ohms) is called the two-dimensional resistivity, sheet resistance, or resistance-per-square. In many thin film applications, one does not know the film thickness or resistivity only the sheet resistance. The result is independent of the electrode area if the size of the contacts is much smaller than the inner-electrode spacing. The 4-point probe measurements are very reliable and they have been used extensively.

The technique has limitations, however, for as more highly resistive materials are examined, the point contacts are incapable of supplying currents that are high enough to make ΔV readily measurable. Furthermore, necessary input resistance of the voltmeter, which must be greater than the resistance between the two inner probes, become very high. The practical upper limit of resistivity that can be measured by the 4-point probe technique is about $10^8 \Omega\text{-cm}$.

4.1.2 The Van der Pauw method

The Van der Pauw method is a technique for doing 4-probe resistivity and Hall effect measurements [4.2]. In essence it provides all easy way to measure.

- Sheet resistivity/ conductivity
- Hall voltage
- Hall mobility

From this one can conclude:

- The resistance/conductance provided the thickness of the sample is known
- Sheet carrier density provided the thickness of the sample is known

The contacts are on the boundary on the surface. The advantages of this method also include its low cost and simplicity. The Van der Pauw technique can be used on thin sample of material and the 4 contacts can be placed anywhere on the perimeter/boundary, provided certain conditions are met as given hereunder:

- The contacts should be on the boundary of the sample (or very close to the boundary as possible)
- The contact should be sufficiently small (or as close as possible)
- The sample is to be homogeneous and thin relative to the other dimensions.
- The surface of the sample is to be singly connected, i.e., the sample does not have isolated holes.

Fig. 4.3 shows the four contacts on the circumference of the disc shaped (irregular shaped) sample. For a fixed temperature, we define resistance $R_{AB,CD}$ as the potential difference is $V_D - V_C$ between the contacts D and C per unit current I_{AB} through the contacts A and B. The current enters the sample through the contact A and leaves it through the contact B.

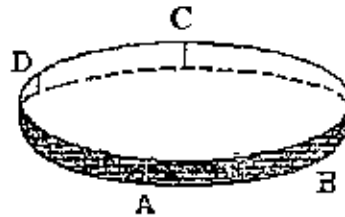


Fig 4.3: The four electrical contacts on the circumference of the rectangular shaped samples.

Then

$$R_{AB,CD} = \frac{V_D - V_C}{I_{AB}} \quad 4.5$$

Analogously we define:

$$R_{BC,DA} = \frac{V_A - V_D}{I_{BC}} \quad 4.6$$

Van der Pauw method is based on the theorem that between $R_{AB,CD}$ and $R_{BC,DA}$ there exists the simple relation:

$$\exp\left(-\frac{\pi d}{\rho} R_{AB,CD}\right) + \exp\left(-\frac{\pi d}{\rho} R_{BC,DA}\right) = 1 \quad 4.7$$

where d is the thickness of the uniform disc shaped sample and ρ is the resistivity of the material. If d and the resistances $R_{AB,CD}$ and $R_{BC,DA}$ are known, then in Eq. 4.7, ρ is the only unknown quantity.

4.2 Impedance and permeability measurement

For the measurement of Impedance and Permeability, Agilent 4294A (frequency 75 KHz to 110 MHz) impedance analyzer has been used. This impedance analyzer has different modes for different measurements. For the impedance measurement the analyzer was connected to a impedance measurement test head and for the measurement of the permeability and inductance the analyzer was connected to a magnetic material test head. In all cases the analyzer with the test head was first calibrated with a standard valued specimen provided from the source of the analyzer.

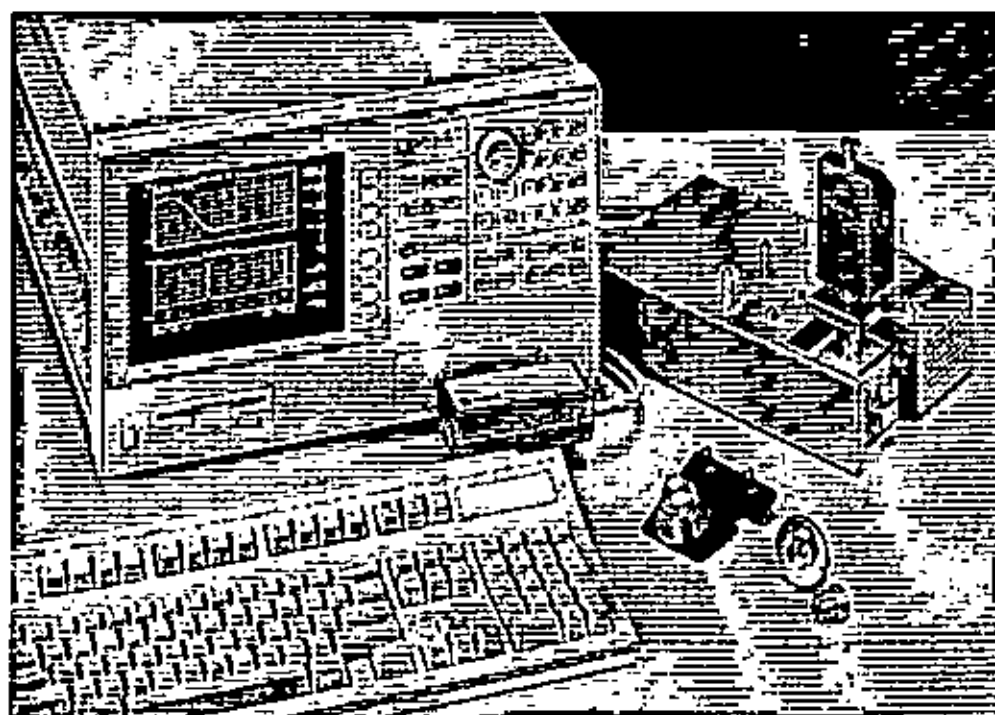


Figure 4.4: Agilent 4294A Impedance Analyzer for magnetic and Dielectric measurement

4.3 Heat diffusivity measurement

A new device is produced for the measurement of heat diffusivity. A glass made funnel is used as a main chamber in which the measurement specimen is retained. A bar of ebonite material is used as a substrate of the specimen. The specimen shape is a rectangular lamina of dimension $15 \times 1.3 \text{ mm}^2$. In the two rectangular ends, hot ends of two thermocouples are placed. The other ends of the thermocouples are kept in ice outside the chamber, which is the 0°C reference. In one end of the specimen there is an electrical device that generates large amount of heat. The whole chamber is evacuated by a rotary pump. Under evacuated

condition heat pulse is given for a certain period of time at one end. The temperatures of the both ends are recorded with time until the both end arrive at the same temperatures. The thermo emf change rate is calculated from the time base temperature curve of the both end from which the thermal diffusivity of the specimen is measured.

The following figure shows the schematic of the device used for this purpose

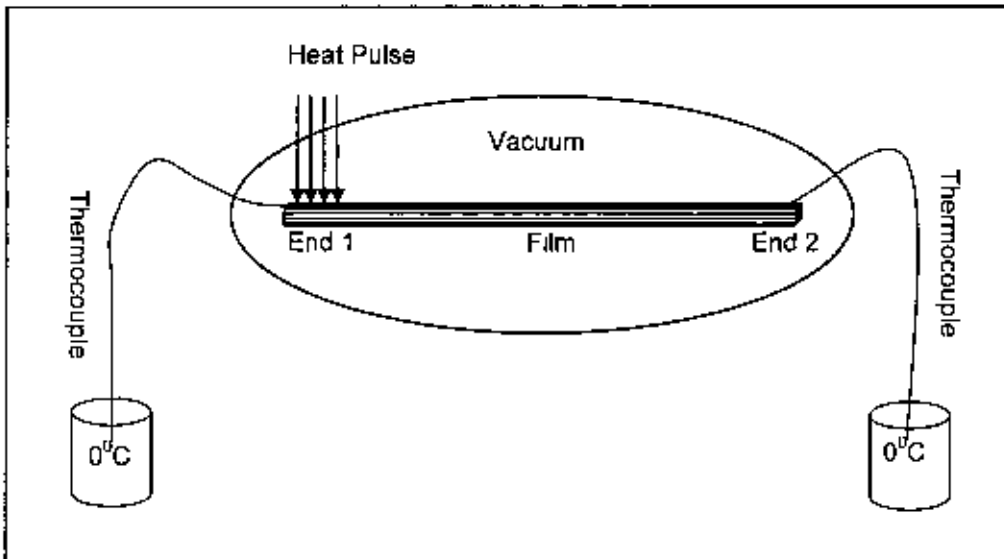


Figure 4.5: Experimental diagram for heat diffusivity Measurement

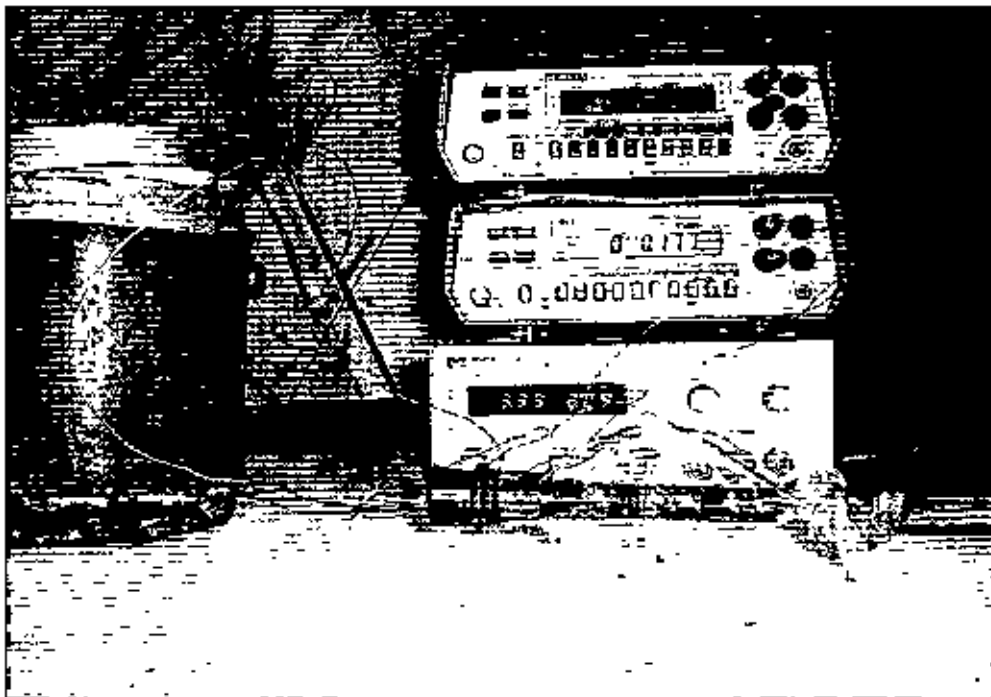


Figure 4.6: Device arrangement for heat diffusivity measurement

4.4 Scanning Electron Microscope

Hitachi S-3400N Variable Pressure Scanning Electron Microscope is used for grain morphology and microstructural characterization equipped with EDS system.

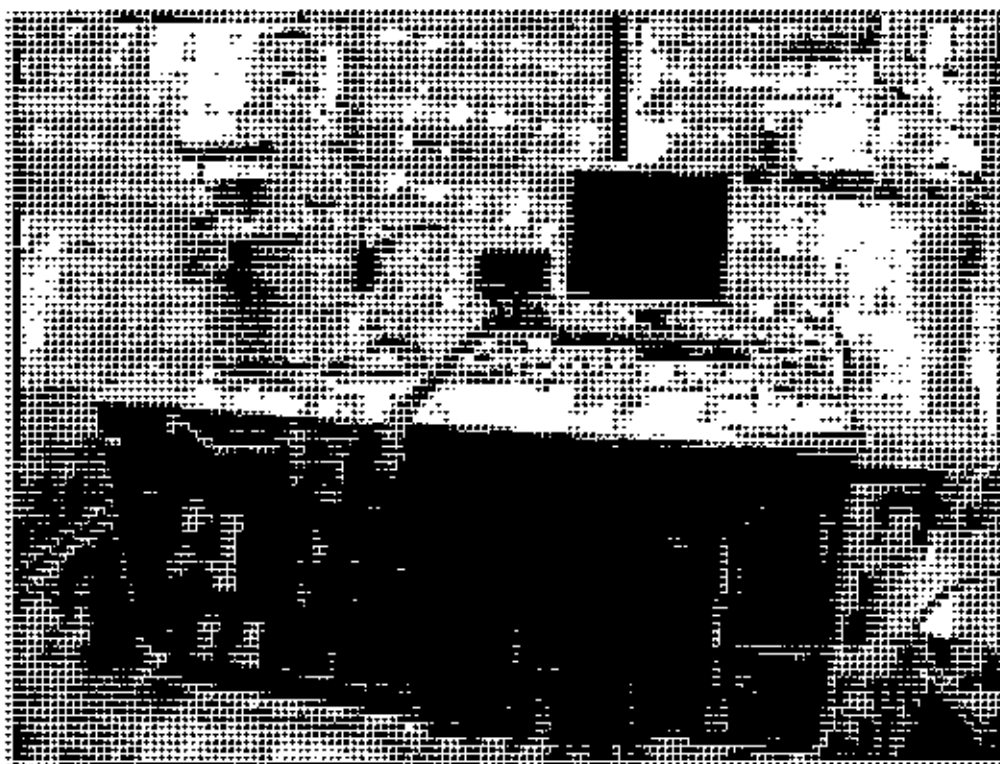


Fig 4.7: External view of Hitachi S-3400N Scanning Electron Microscope

4.5 DTA, TGA and DTG measurement

For the investigation of thermal response of the film we have taken DTA, TGA and DTG of the film. For this purpose we have used the lab facility of Bangladesh Council of Scientific and Industrial Research, Dhaka

Chapter Five

Results and Discussion

5.1 Micro structural Characteristics

The magneto-transport and the structural properties of $(\text{Fe}_{100-x}\text{V}_x)_{75}\text{P}_{15}\text{C}_{10}$ have been measured as a function of temperature, magnetic field and frequency. The electron diffusivity properties of the samples have also been investigated through time decay of monochromatic light pulse. The structural properties have been investigated through SEM, DTA, TGA and the EDS measurements. The electrical properties and the magnetic transport properties have been investigated through measurements of electrical resistivity and the magnetoresistance properties of the material.



Fig-5.1(a) SEM micrographs of sample-1 ($x=1.5$)

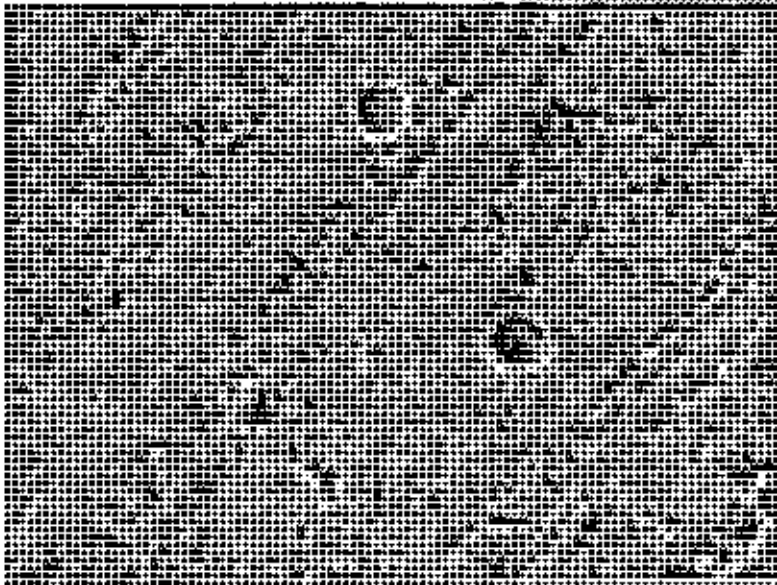


Fig-5.1(b): SEM micrographs of sample-2 ($\times 3$)

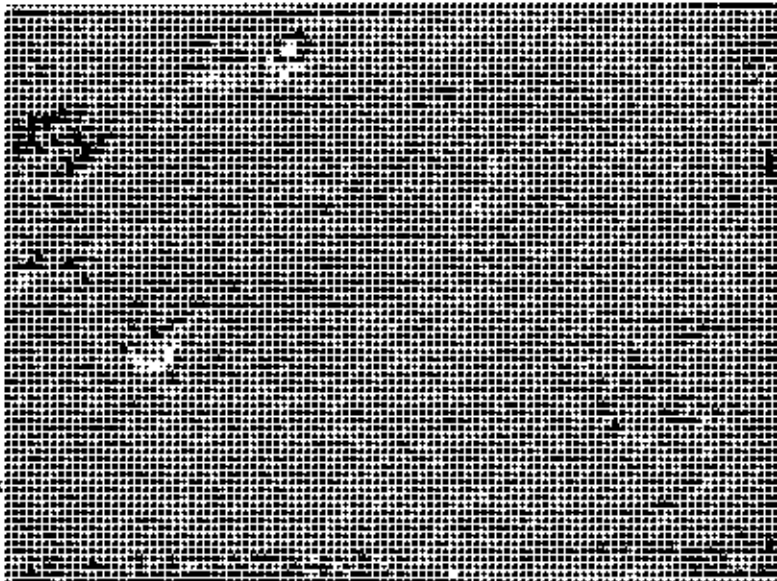


Fig-5.1(c): SEM micrographs of sample-3 ($\times 9$)

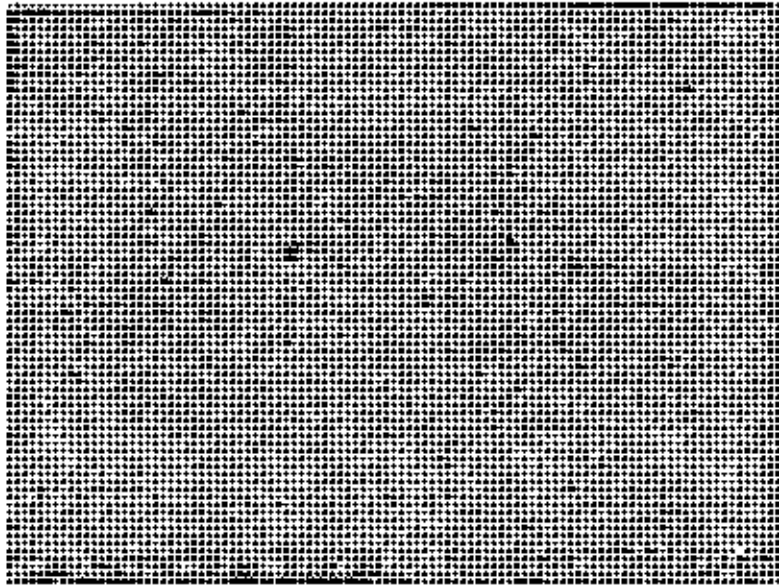


Fig-5.1(d): SEM micrographs of sample-4 (x=15)

SEM images show a uniform surface texture of the samples. Further details about the surface morphology could not be studied because of the low resolution of the SEM machine. It is assumed that the microstructure contains well defined grain boundaries and that the grains got smaller in size with annealing. The critical balance between saturation magnetization and the grain size is well recognized through the magnetization data and the subsequent DTA and TGA analysis. The balance between grain size and the saturation magnetization is governed by D^6 law where D is the diameter of the particle. When D approaches 10-20 nano-meter in size then the material shows its novel soft magnetic properties. The replacement of Fe with V is to induce some magnetic coercivity in the material. With proper precision measurements of hysteresis it is possible to see this feature. The addition of V to Fe would reduce the magnitude of saturation magnetization. However, a subsequent hysteresis loop broadening should reveal that the magnetic coercivity has increased due to the addition of V.

5.2 EDS Spectra

The EDS detector measures emitted X-rays versus their energy. The energy associated with the emitted X-ray is characteristic of the element from which the X-ray emitted. A spectrum of the energy versus relative counts of the detected X-rays is obtained and evaluated for qualitative and quantitative determinations of the elements present in the sampled volume. On this work EDS Spectra pattern of the samples were taken at room temperature using a Hitachi S-3400N EDS machine. Samples analyzed by X-ray fluorescence are shown in Fig-5.2 (a-d).

Full scale counts: 3001

■ Sample 1
■ Synthetic Spectrum

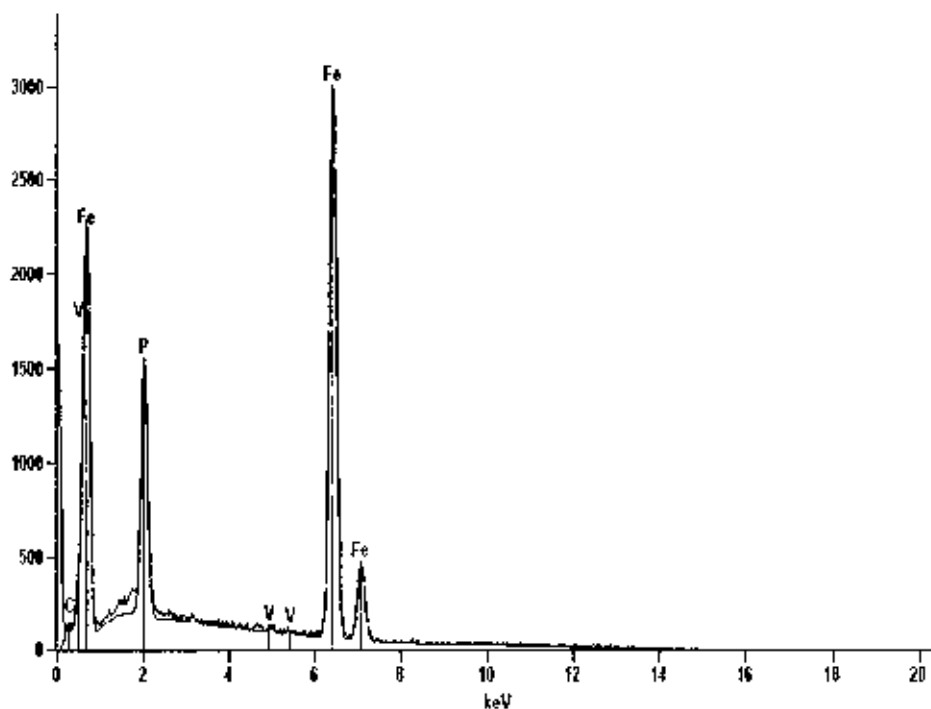


Fig-5.2(a): EDS Spectrum of sample-1 (x=1.5)

Full scale counts: 3000

■ Sample 2
■ Synthetic Spectrum

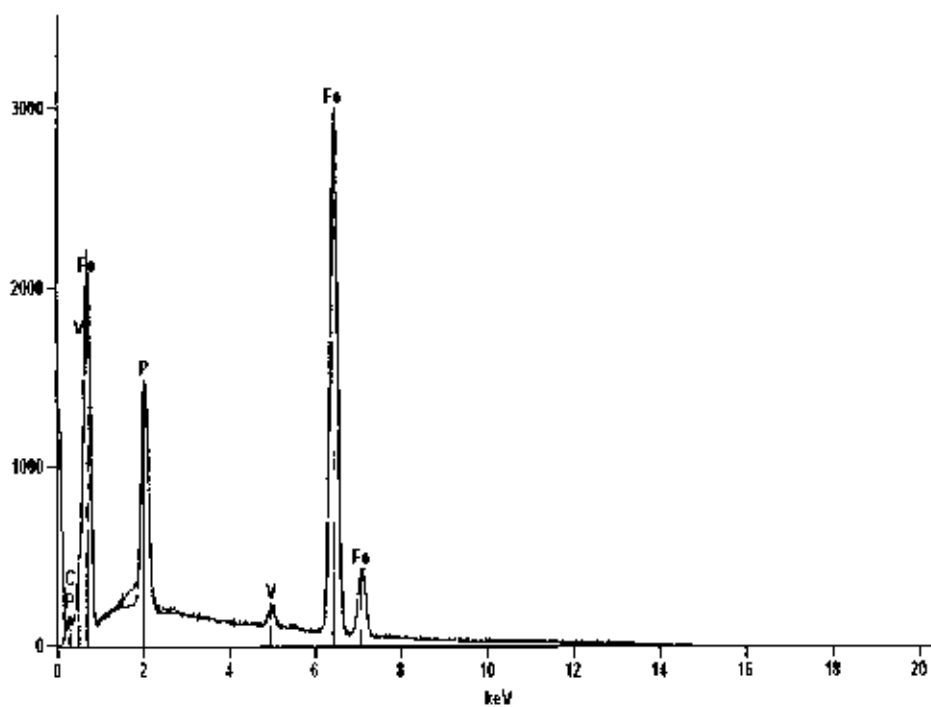


Fig-5.2(b). EDS Spectrum of sample-2 (x=3)

Full scale counts: 3000

Sample 3
■ Synthetic Spectrum

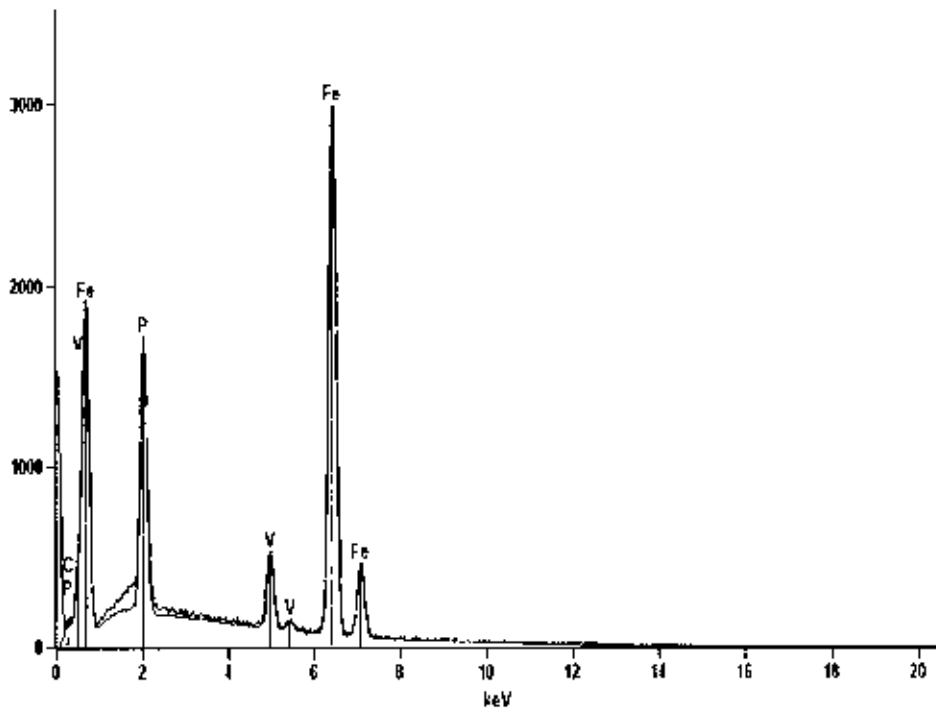


Fig-5.2(c). EDS Spectrum of sample-3 (x=9)

Full scale counts: 3000

Sample 4
■ Synthetic Spectrum

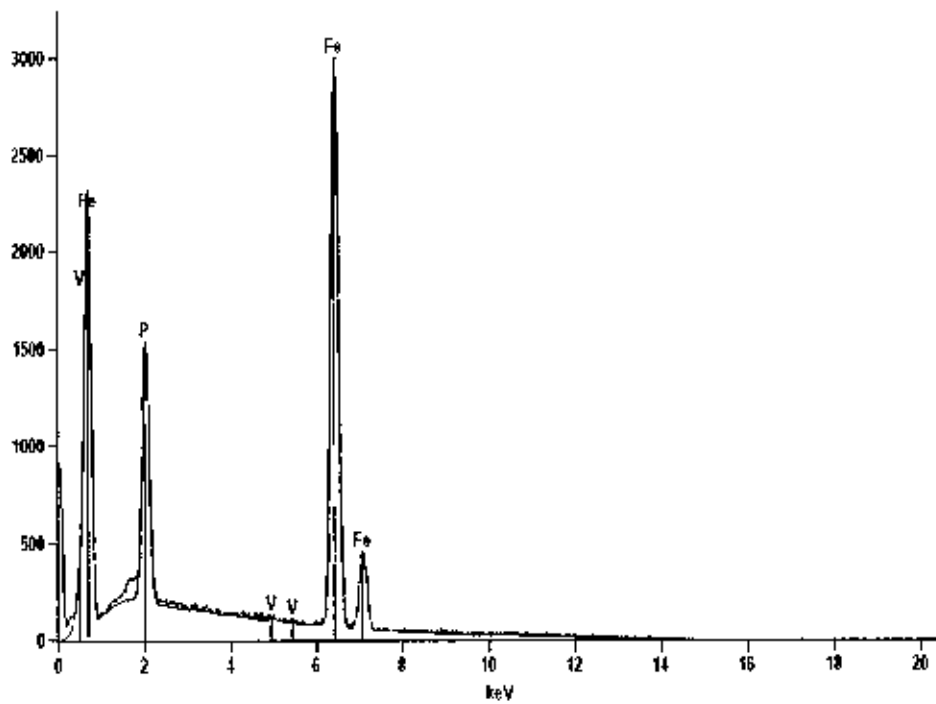


Fig-5.2(d) EDS Spectrum sample-4 (x=15)

Table-1: Semi-quantitative weight %

Sample	Fe	V	P	C
(Fe _{98.5} V _{1.5}) ₇₅ P ₁₅ C ₁₀	87.17	0.23	8.40	4.20
(Fe ₉₁ V ₉) ₇₅ P ₁₅ C ₁₀	84.36	1.85	8.23	5.56
(Fe ₇₁ V ₉) ₇₅ P ₁₅ C ₁₀	79.94	6.23	8.49	5.34
(Fe ₈₅ V ₁₅) ₇₅ P ₁₅ C ₁₀	77.23	7.84	8.53	6.40

From the above EDS spectra and table we observed that all the elements of the test samples are present in their proportional form. Therefore no elemental loss was detected from this study. There is however a slight change in the composition due to the presence of micro-voids mainly occupied by air which has formed some oxides upon annealing at higher temperature. These oxides are again eliminated upon annealing at even higher temperature around the crystallization temperature T_c . One of the studied samples has shown anomalous behavior of rapid enhancement in magnetization values for higher V content. The role of V in this particular case is contrary to the case for smaller V content where it was predicted that V only helps in grain growth. In this case the higher V content is thought to have enhanced the growth kinetics of nano-grain formation. This is revealed by the abrupt enhancement in magnetization of the sample for higher V content.

5.3 The Impedance Measurement

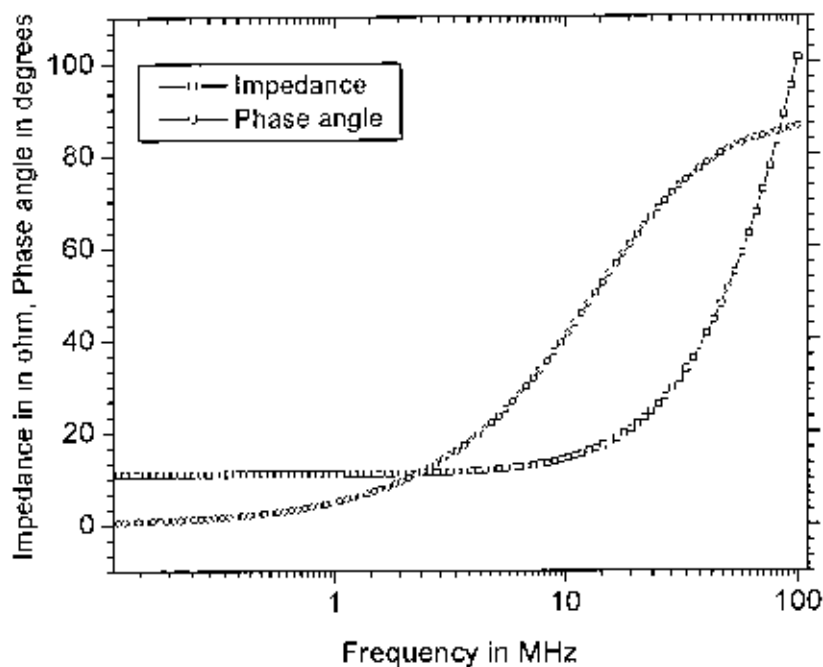


Figure 5.3(a) : Variation of Impedance and phase angle with frequency for Sample-1(x=1.5)

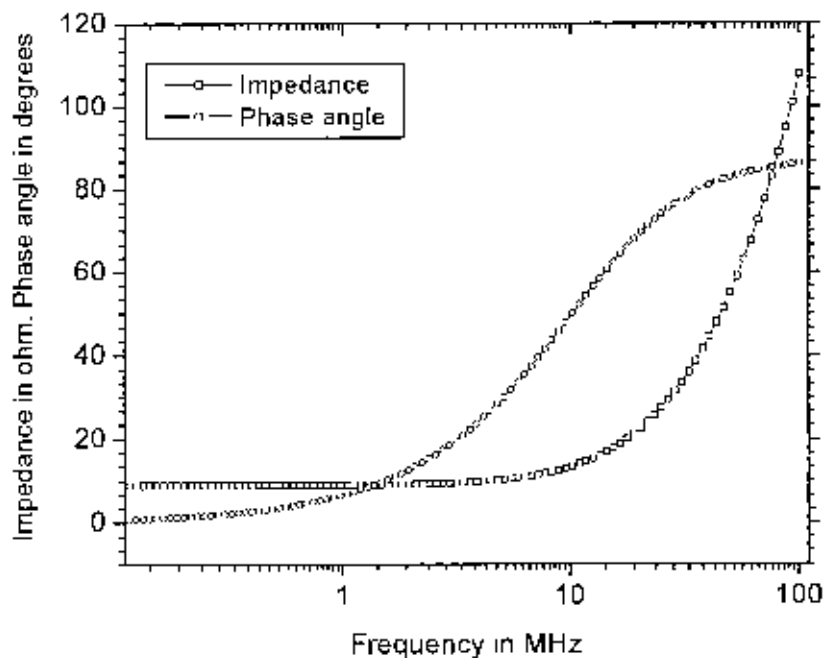


Figure 5.3(b) : Variation of Impedance and phase angle with frequency for Sample-2 (x=3)

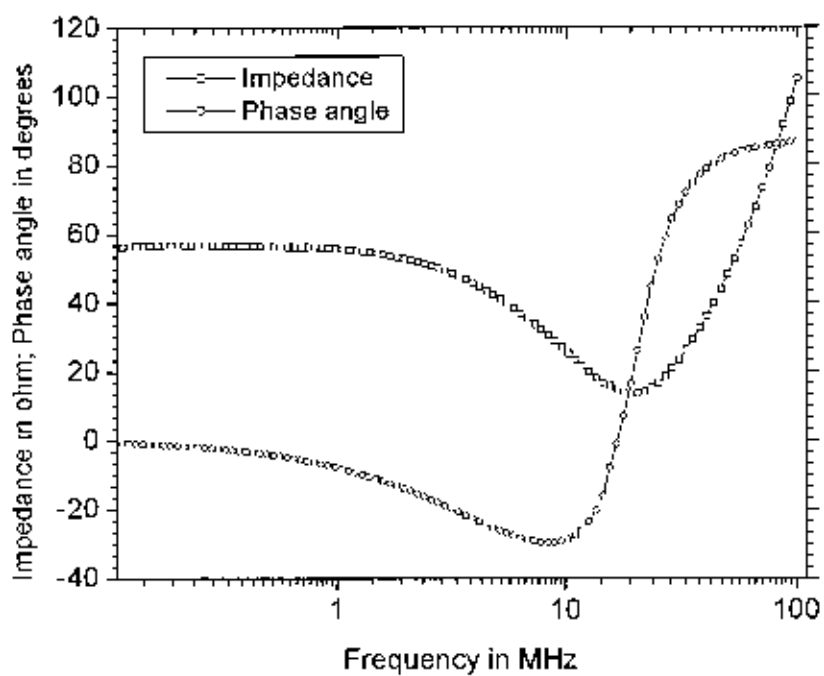


Figure 5.3(c) : Variation of Impedance and phase angle with frequency for Sample-3 (x=9)

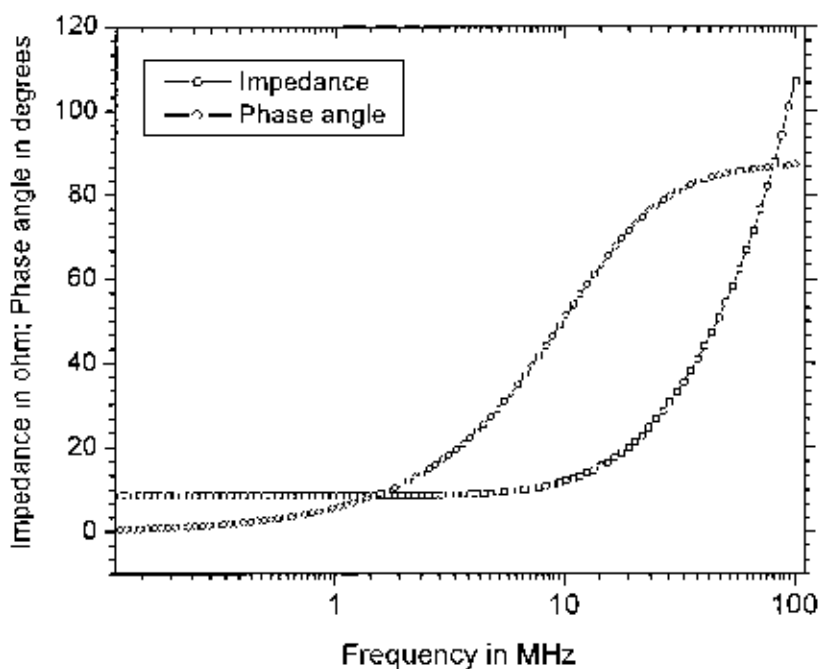


Figure 5.3(d) : Variation of Impedance and phase angle with frequency for Sample-4 (x=15)

Figure 5.3 shows the impedance and the corresponding phase angle at different frequencies. The frequencies of measurements were set up between 40 Hz to 110 MHz. The impedance remained constant upto a certain frequency and has shown remarkable increase afterwards. This behavior limits the frequency range upto which the samples could be used in ac circuits. In this case the impedance remained constant upto 10 MHz afterwards it began to increase with increasing frequency reaching a maximum at 110 MHz. Similarly phase angle increases with the increases of frequency. It seems that after 100 MHz the phase angle reached a maximum and then saturated around the same frequency. In Fig 5.3(c) we observed that impedance remain constant up to 1 MHz then decreases with frequency and minimum at 10.1 MHz thereafter sharply increases and reached maximum at 100 MHz. Similarly phase angle decreases with frequency up to 10 MHz then increases with frequency and reached to saturation after 30 MHz. Fig 5.4 shows the electrical resistivity of the measured samples as a function of temperature. All the samples show a drop in resistivity above 500 K which is close to the glass transition temperature T_g , the onset of crystallization with the crystallization temperature T_x being always higher than T_g . At higher frequency samples show a semiconductor behavior.

5.4 High Temperature Measurement

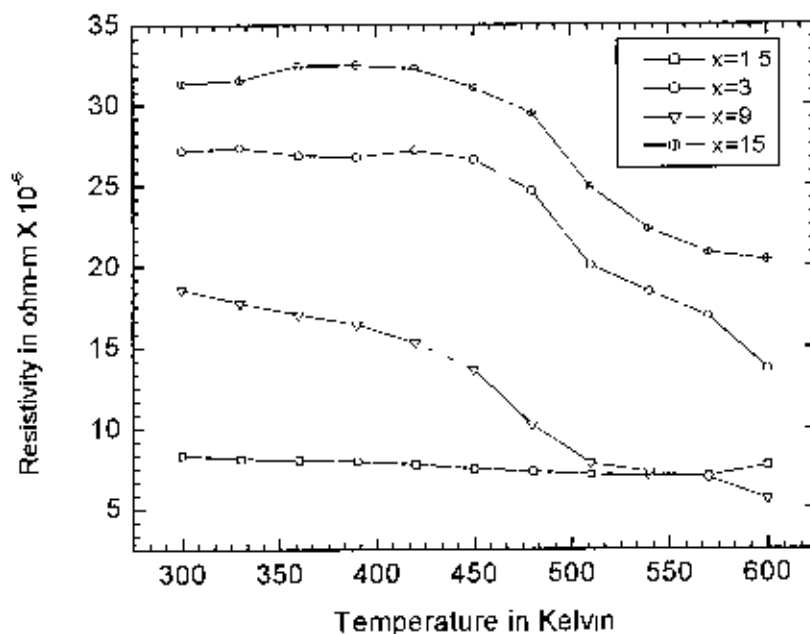


Figure 5.4: Resistivity vs Temperature Curve for Different samples

Fig-5.4 shows the resistivity measurement with temperature. Here we observed that resistivity remains constant upto 450 K thereafter decreases. The decrease in electrical resistivity around 450K corresponds to the onset of micro-crystallites formation. The process continues upto the crystallization temperature T_x where the resistivity shows a sharp fall and the more ordered crystalline structures are expected to have formed around this temperature. This temperature also corresponds well the magnetic phase transition temperature T_c where the sample enters into the paramagnetic phase. The reversibility of the phase transformation is not expected as typical for other metallic glass system in which there is usually a thermo-magnetic hysteresis when the temperature is reduced to re-enter into the ferromagnetic phase. In this study a similar thermo-magnetic hysteresis formation is predicted. The thermo-magnetic hysteresis is a measure of the energy stored in the system when thermal switching is done. This is a typical behavior of conventional metallic glasses since the order-disorder mechanism is governed on the basis of the growth process during melt-spinning.

5.5 Magnetoresistance Measurement

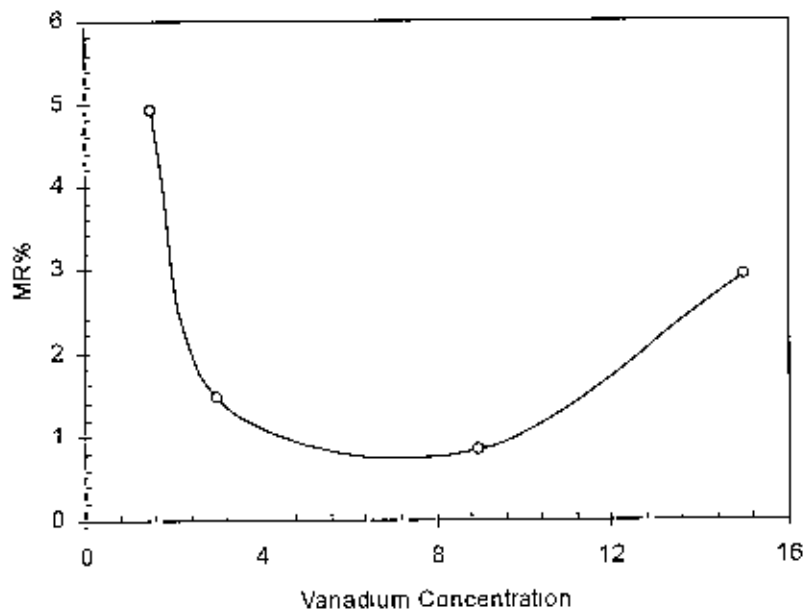


Fig-5.5: Variation of MR% with different Vanadium concentration

Fig-5.5 shows the MR% at room temperature for different Vanadium (V) concentration. It is seen from the figure that MR% decreases with increases of Vanadium concentration up to 9 at% thereafter it increases. The possible reason may be attributed to the formation of nano-grains initiated by vanadium at higher concentration. This enhancement in MR% has been supported by the magnetization data which has also shown a remarkable increase in the magnetoresistance value for this particular concentration of V. The magnetoresistance is governed by the electron spin-scattering centers. During the demagnetization process the magnetic domains and the conduction electron scatterings take part to contribute to the electrical resistivity and the magnetoresistance. Once the magnetic saturation is achieved there is no domain motion as it has assumed a single domain. The only contribution to the electrical resistivity and the magnetoresistance comes at this stage is from the conduction electron scattering due to the collision between themselves and the electron mean free-path is much longer in this stage. The temperature coefficient during the demagnetization process is usually negative. The only reason for this negative TCR is the longer free-path of the electron and there is no scattering of the conduction electrons from the domain boundaries.

5.6 Permeability Measurement

For the measurement of Permeability, Agilent 4294A (frequency 40 Hz to 110 MHz) impedance analyzer has been used. Frequency was set up from 40 Hz to 100 KHz as at higher frequency permeability remain constant.

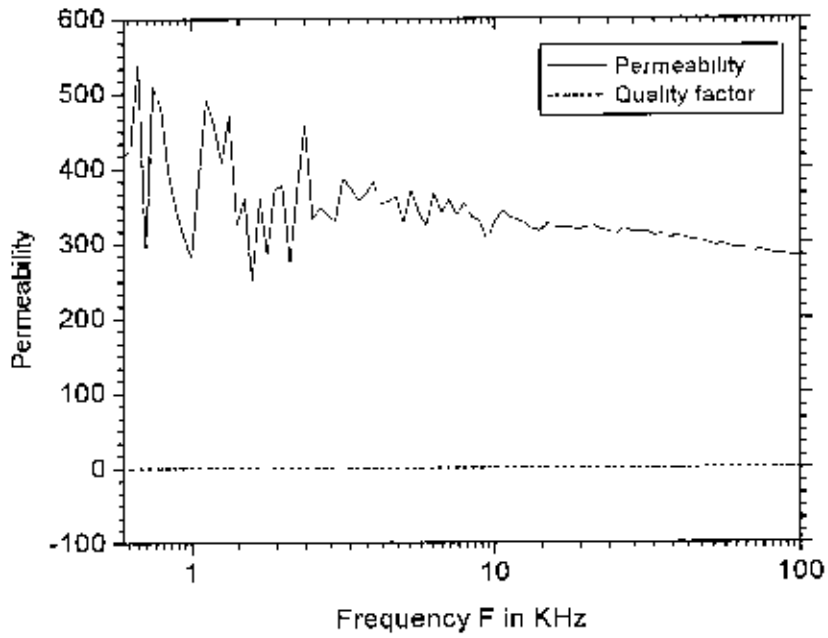


Fig-5.6(a): Variation of Permeability and Quality factor with frequency for sample-1 ($x=1.5$)

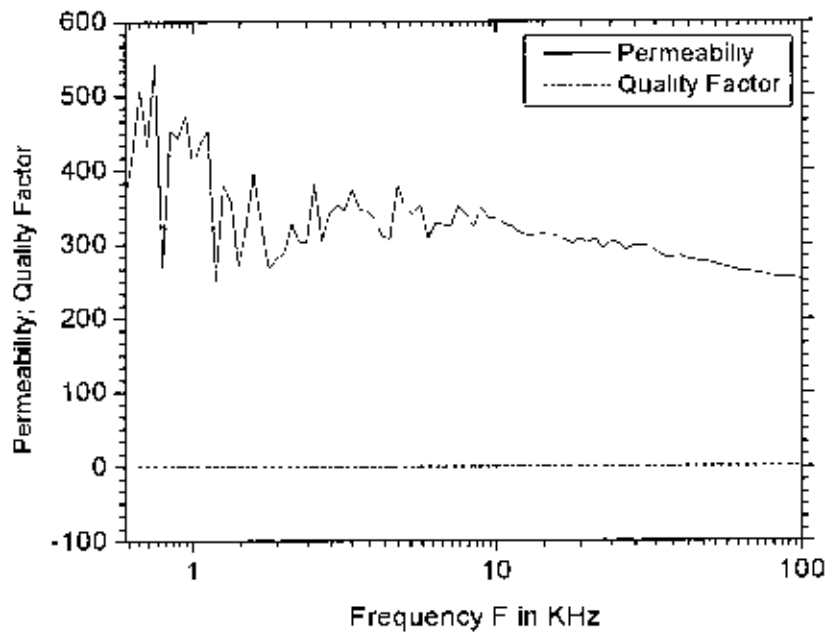


Fig-5.6(b): Variation of Permeability and Quality factor with frequency for sample-2 ($x=3$)

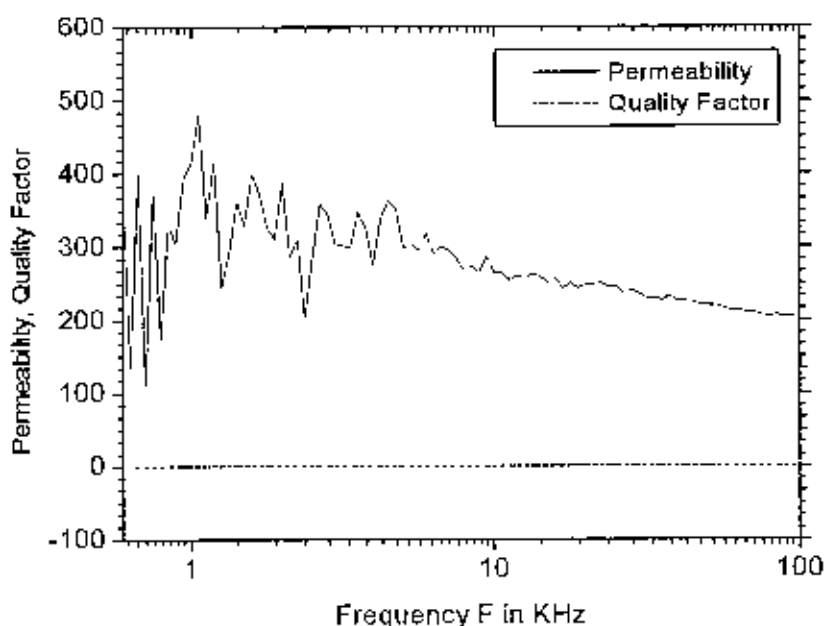


Fig-5.6(c): Variation of Permeability and Quality factor with frequency for sample-3 ($x=9$)

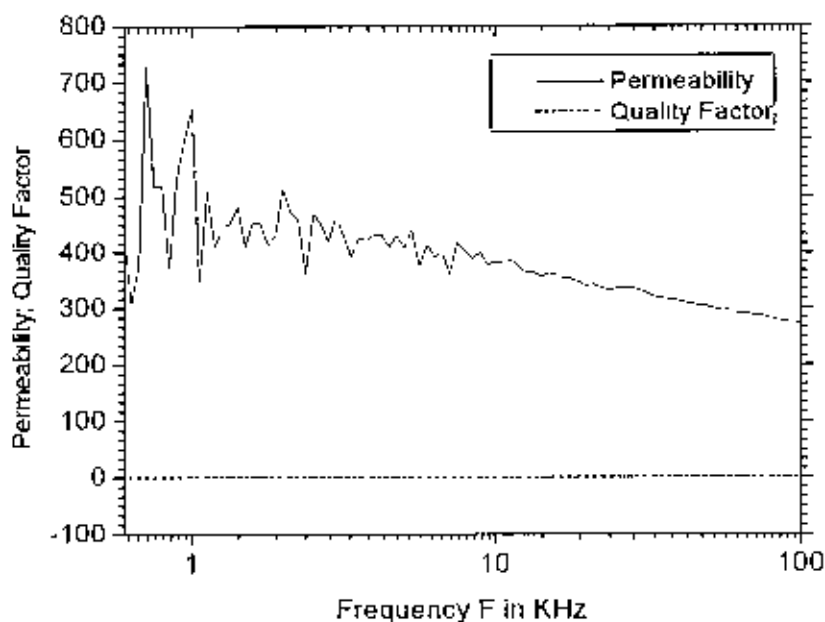


Fig-5.6(d): Variation of Permeability and Quality factor with frequency for sample-4 ($x=15$)

Fig-5 6(a-d) shows the permeability of the specimen material at different frequencies. The a c permeability studies show a systematic decrease in the a c magnetic response of the samples with increasing frequency. Some resonance peaks are found near 1 KHz that means that magnetization will be maximum on that particular frequency. Quality factor remains constant with increasing of frequency.

5.7 The Magnetization Measurement

The magnetization measurement of the films was done to observe its magnetic property.

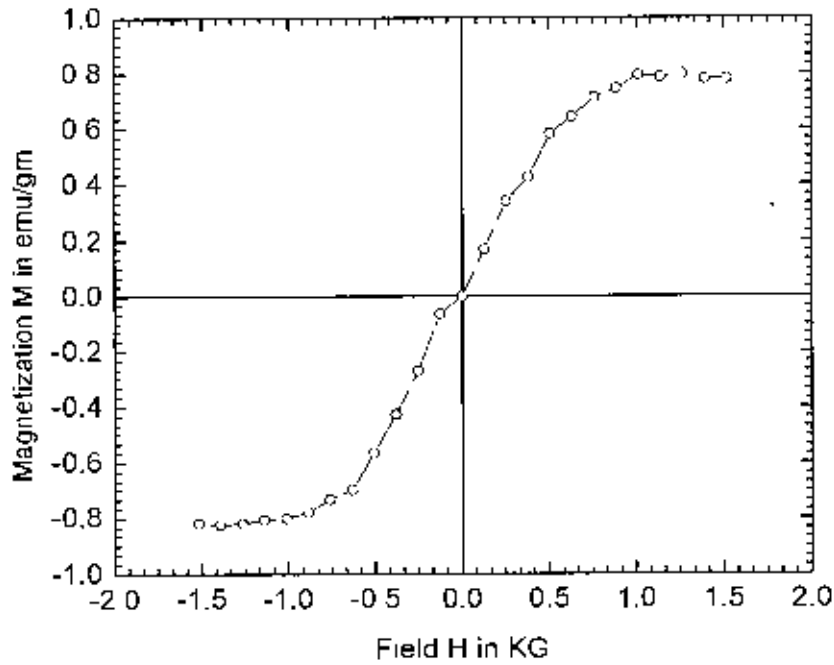


Fig- 5.7(a): Magnetization curve for direct and reverse field for sample-1($x=1.5$)

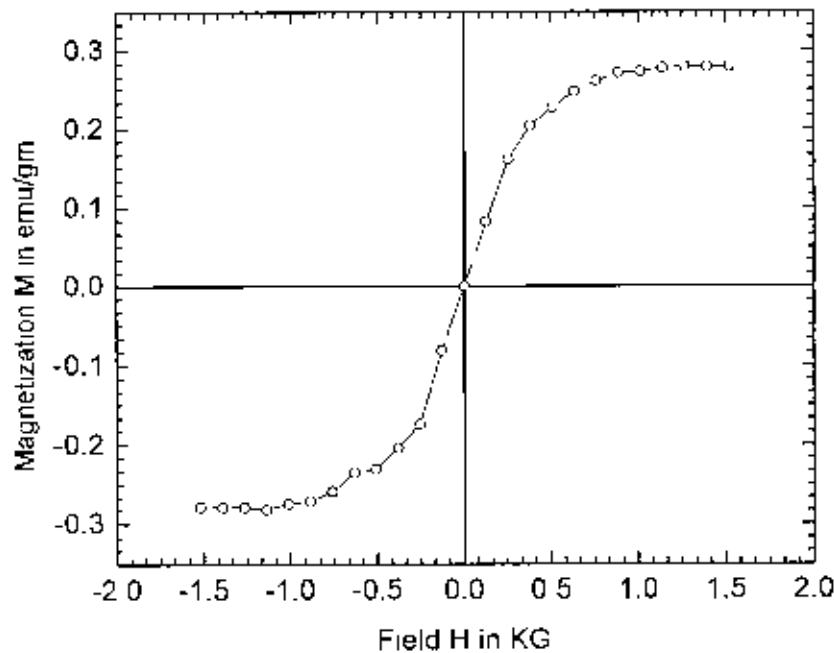


Fig- 5.7(b): Magnetization curve for direct and reverse field for sample-2 ($x=3$)

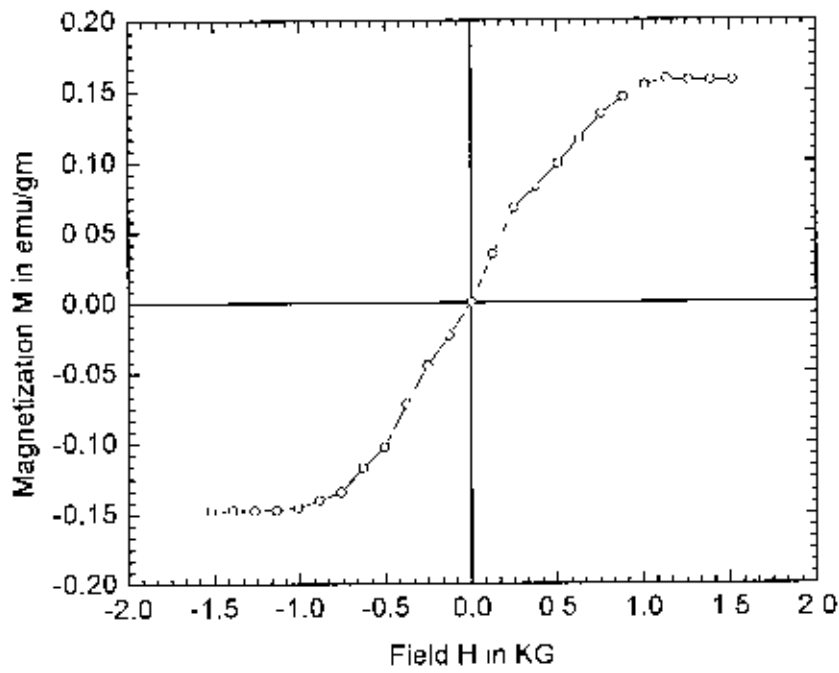


Fig- 5.7(c): Magnetization curve for direct and reverse field for sample-3 ($x=9$)

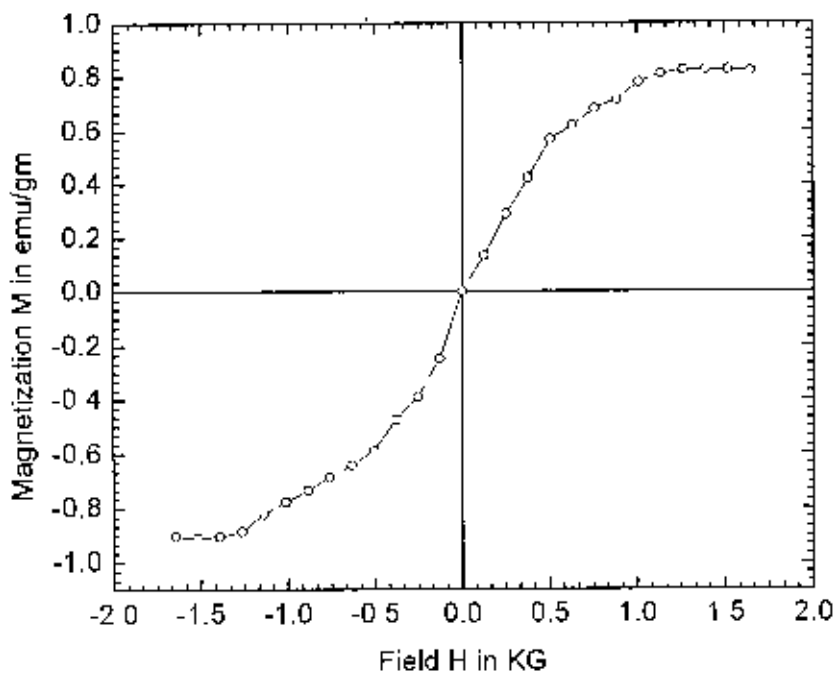


Fig- 5.7(d): Magnetization curve for direct and reverse field for sample-4 ($x=15$)

Table-2. Data for Saturation Magnetizaion of the samples

Sample	Sat Magnetization [a.u]
Sample-1, x=1.5	0.8
Sample-2, x=3	0.27
Sample-3, x=9	0.15
Sample-4, x=15	0.08

From the study of magnetization we found that the addition of Vanadium (V) has resulted in significant decrease in magnetization values. Addition of V is likely to have increase in grain size in a matrix of ferromagnetic Fe particles surrounded by the non-magnetic C and P atoms. However, an exceptional behavior was recorded for the sample-4 (x=15) which has shown a remarkable increase in magnetization values. The possible reason for this unusual behavior may be attributed to the formation of nano grains initiated by vanadium. This enhancement in magnetization has been supported by the magnetoresistance data which has also shown a remarkable increase in the magnetoresistance value for this particular concentration of V.

107245

5.8 DTA, TGA, DTG Analysis

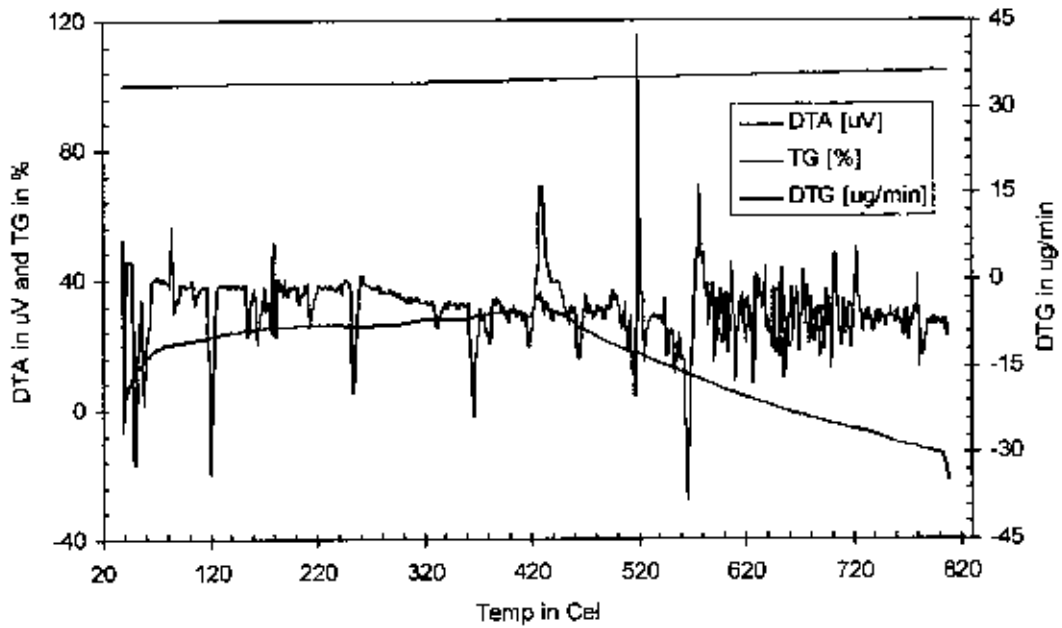


Fig-5.8(a): DTA, DTG and TG Curve for Sample-1 (x=1.5)

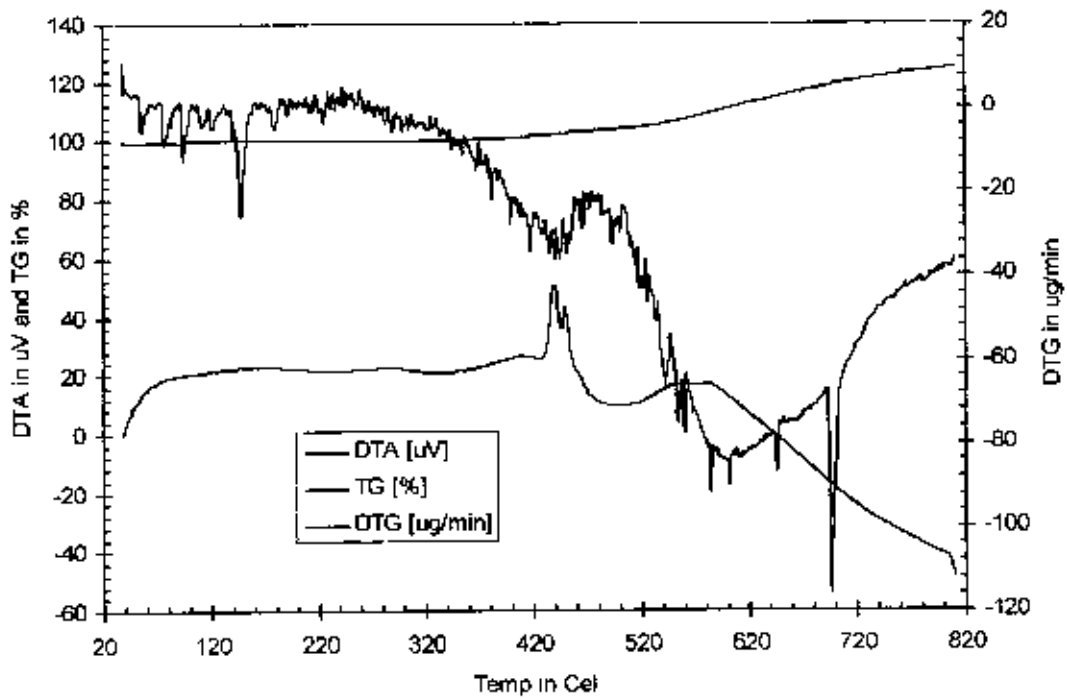


Fig-5.8(b): DTA, DTG and TG Curve for Sample-2 (x=3)

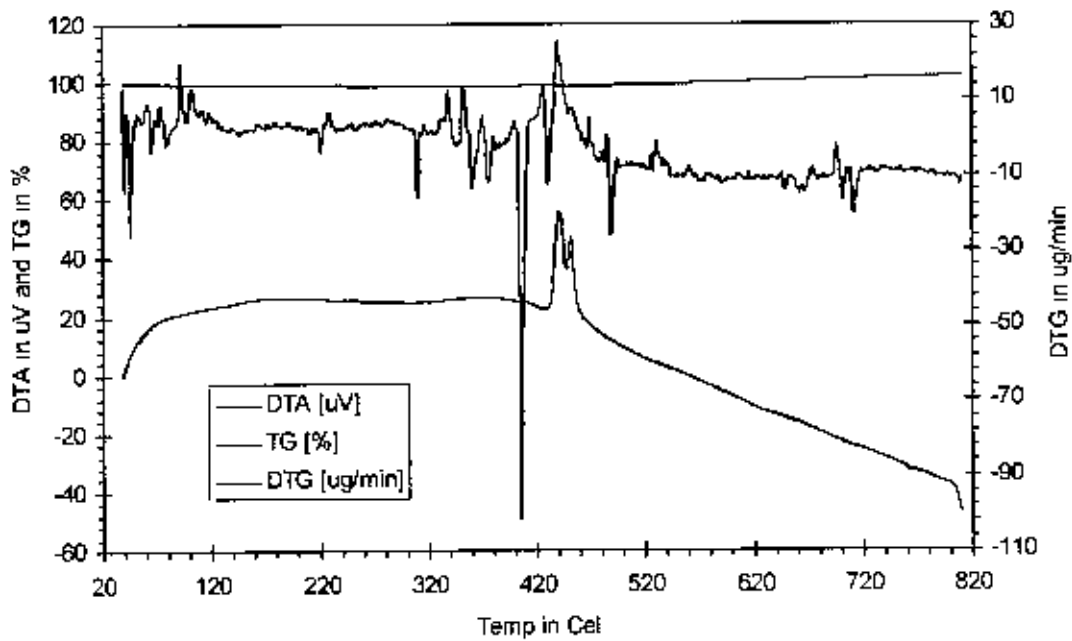


Fig-5.8(c): DTA, DTG and TG Curve for Sample-3 (x=9)

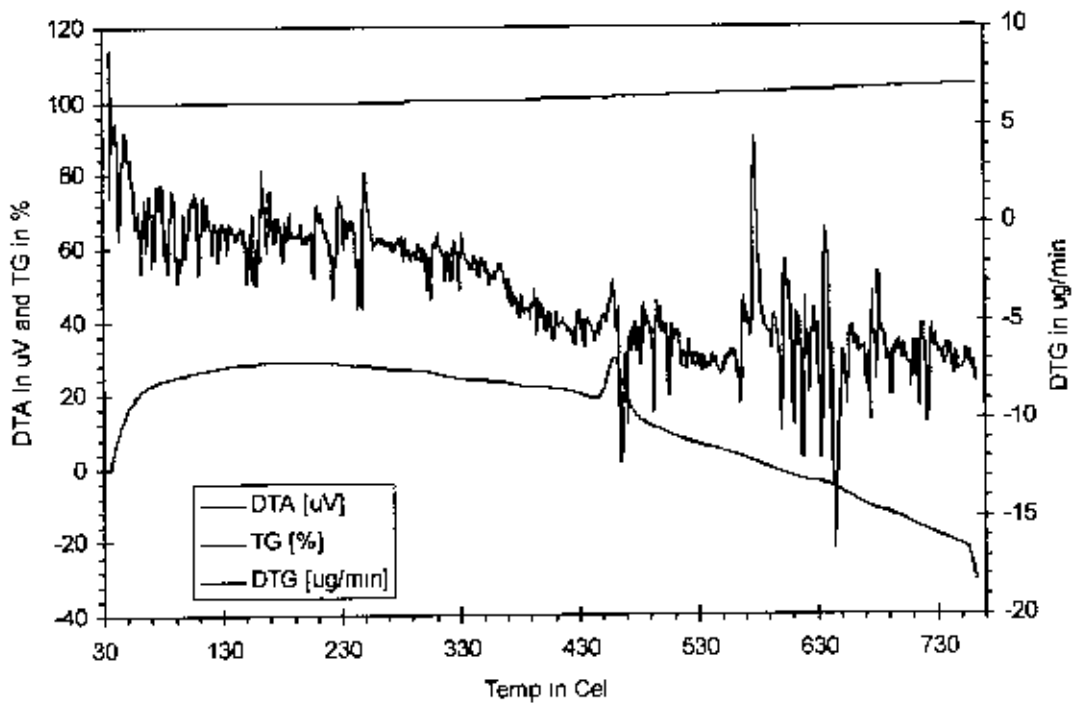


Fig-5.8(d): DTA, DTG and TG Curve for Sample-4 (x=15)

Figure 5.8(a-d) shows the differential thermal analysis (DTA), thermo-gravimetric analysis (TGA) and differential thermo-gravimetric (DTG) of the films

DTA: In the DTA curve two exothermic rise is occurred for sample 1, 2 and 3 and one exothermic rise is occurred for sample 4 The peak values are given in the table below

Table-3: DTA peak values of the different samples

Sample	1 st Peak (°C)	2 nd Peak (°C)
Sample-1	429.6	445.9
Sample-2	439.6	449.5
Sample-3	440.2	451.3
Sample-4	460.8	---

The first peak attributed to the structural phase transformation and second one attributed to oxidation at higher temperature

TG %: In the TG % curve we observed that mass is slightly gained in all samples As temperature is increased the micro voids which formed during the growth process of the ribbon during melts spinning is gradually eliminated. This results in densification of the matrix of the more ordered crystallites in the samples at higher temperature.

5.9 Heat Diffusivity Measurement

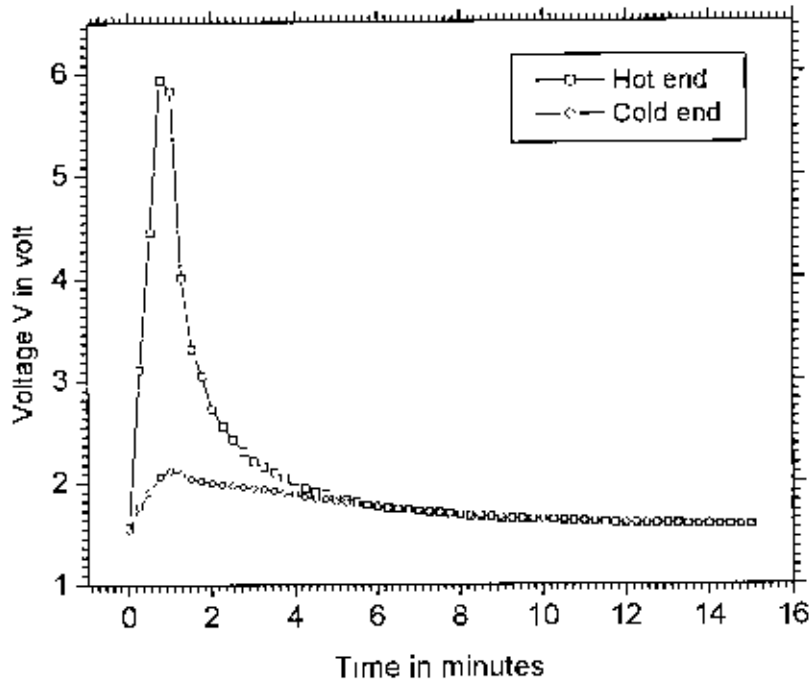


Fig- 5.9(a): Variation of thermal emf with time at hot end & cold end for sample-1

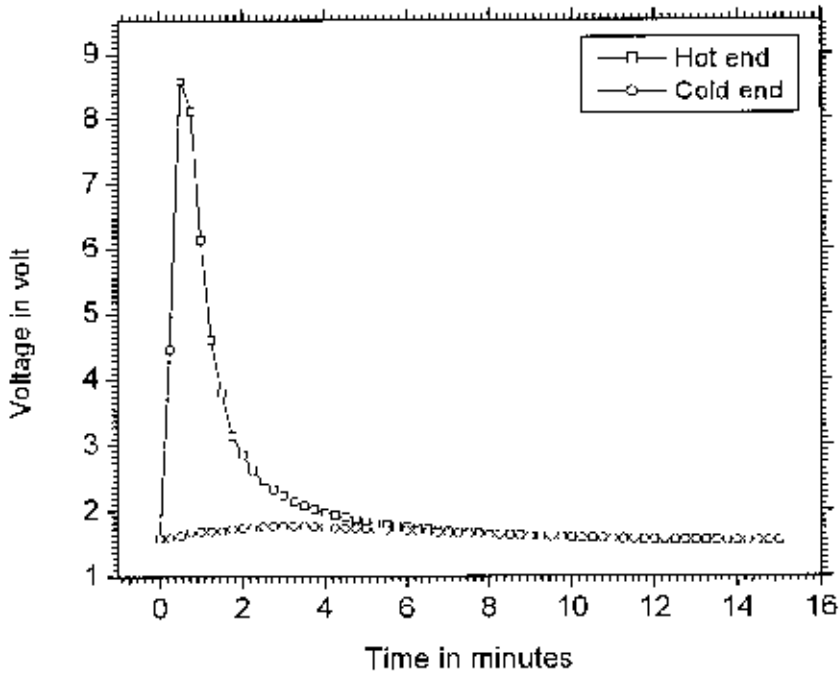


Fig- 5.9(b): Variation of thermal emf with time at hot end & cold end for sample-2

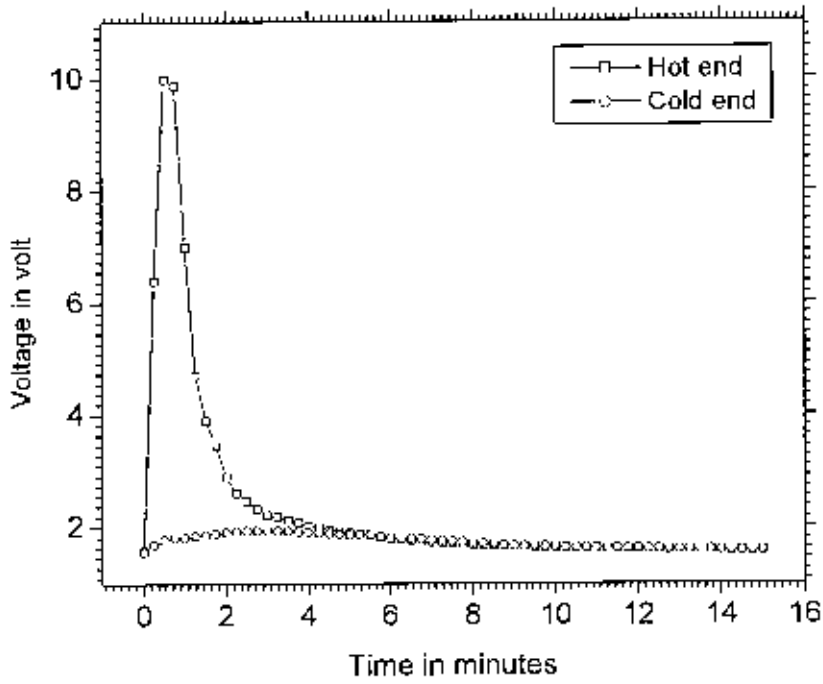


Fig- 5.9(c): Variation of thermal emf with time at hot end & cold end for sample-3

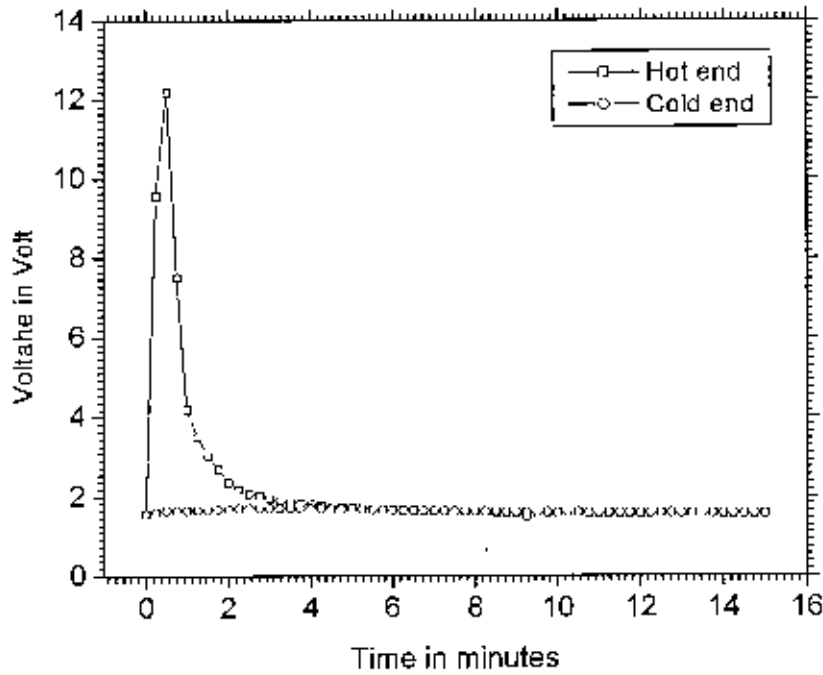


Fig- 5.9(d): Variation of thermal emf with time at hot end & cold end for sample-4

Figure 1(a-d) shows the heat diffusivity measurement curves. The two curves indicate the temperature rise and fall of the hot and cold end respectively. The diffusivity is measured from the temperature curve of the cold end by the formula

$$\alpha = \frac{0.139A^2}{t_{50}} \text{ m}^2/\text{sec}$$

Where t_{50} is the half rise time of the cold end and A is the area of cross section of heat diffusivity.

Table-4: Calculated values of heat diffusivity for different samples

Sample	Heat diffusivity α in $\text{m}^2/\text{sec} \times 10^{-11}$
Sample-1	4.633
Sample-2	1.425
Sample-3	1.684
Sample-4	1.544

From the heat diffusivity measurement we observed that typical value is similar with metallic glass.

Chapter Six

Conclusion and Future Work

6.1 Conclusion

The magnetic and structural properties of $(\text{Fe}_{100-x}\text{V}_x)_{75}\text{P}_{15}\text{C}_{10}$ ($x=1.5, 3, 9, 15$) alloys have been studied by measuring the magnetization and structural parameters. The samples are fabricated by conventional melt spinning technique at wheel speed of 25 m/sec. The as made samples are found to be ferromagnetic at room temperature and all of them go through the magnetic phase transition around 500-600 K. SEM images show a uniform surface texture of the samples and from the EDS spectra we observed that all the elements of the test alloy are present in their proportional form.

The impedance measurements on all the samples show a pronounced non linearity above 10 MHz with the exception of $(\text{Fe}_9)\text{V}_9)_{75}\text{P}_{15}\text{C}_{10}$. Further detailed studies are needed to explain this behavior of the sample.

The magnetic phase transition of all the studied samples are observed to be around the glass transition temperature T_g (650 - 700 K).

The a.c. permeability studies show a systematic decrease in the a.c. magnetic response of the samples with increasing frequency. Some peaks are found near 1 KHz which means that the magnetization will be maximum on that particular frequency. In the quality Factor curve we observed that the Quality factor (Q) is constant with frequency with no loss occurred.

Addition of Vanadium (V) has resulted in significant decrease in magnetization values for all the samples but one. Addition of V is likely to have increased the grain size in a matrix of ferromagnetic Fe particles surrounded by the non-magnetic C and P atoms. However, an exceptional behavior was recorded for the sample $(\text{Fe}_{85}\text{V}_{15})_{75}\text{P}_{15}\text{C}_{10}$ which has shown a remarkable increase in magnetization values. The possible reason for this unusual behavior may be attributed to the formation of nano grains initiated by vanadium. This enhancement in magnetization has been supported by the magnetoresistance data which has also shown a remarkable increase in the magnetoresistance value for this particular concentration of V.

The DTA and TGA data have shown some exothermic peaks above 700 K indicating some structural phase transformation above this temperature. All the studied samples have shown a small second peak at even higher temperature around 800 K which may be

attributed to oxidation of the samples. The EDS analysis shows that addition of V did not cause any stoichiometric imbalance in the alloy system. Addition of V is expected to increase the coercivity of the alloy system and enhance the magnetic properties. However, from this study it is found that the role of V is similar to addition of a non-magnetic solute in a magnetic alloy which is depicted in the magnetization curves of all the studied samples.

6.2 Suggestions for future work

The following experiments can be carried out for understanding the magneto-transport and the structural properties of $(\text{Fe}_{100-x}\text{V}_x)_{75}\text{P}_{15}\text{C}_{10}$

1. Measurement can be done with high resolution of SEM to determine the structure of the samples clearly
2. Temperature dependent magnetic a.c. permeability and magnetization may be measured to determine the Curie Temperature (T_c).
3. XRD can be taken to determine the transformation of samples after DTA and TGA measurement
4. Resistivity is to be measured with low temperature to determine the low temperature behavior of the samples
5. Samples are to be annealed to eliminate the micro-voids.
6. Exceptional behavior was found at 15 at% of Vanadium (V) in magnetization and magnetoresistance measurements so investigation can be carried out around 15 at% of V.

List of Symbols and Nomenclature

A	-	Stiffness Constant
Fe	-	Iron
Cu	-	Copper
Nb	-	Niobium
Ta	-	Tantalum
Si	-	Silicon
B	-	Boron
Co	-	Cobalt
$\rho(RT)$	-	Resistivity at room temperature.
$\rho(T)$	-	Resistivity at any temperature (other than room temperature)
$\frac{\rho(T)}{\rho(RT)}$	-	Normalized resistivity
$\frac{\Delta\rho}{\rho(0)}$	-	Magnetoresistance
MR%	-	Magnetoresistance in percent.
δ	-	Wall width
MI	-	Magnetoimpedance
GMR	-	Giant Magnetoresistance
GMI	-	Giant magnetoimpedance
Z	-	Impedance
R	-	Resistance
X	-	Reactance
QF	-	Quality factor
DF	-	Dissipation factor
L	-	Inductance
L_{ex}	-	Exchange interaction length
μ_0	-	Permeability in free space.
μ_i	-	Initial permeability
μ'	-	Real part of complex permeability
μ''	-	Imaginary part of complex permeability
H_c	-	Coercivity
E_k	-	Anisotropy energy

J_s	-	Saturation magnetization
D	-	Grain diameter
K_u	-	Uniaxial magnetic anisotropy constant
T_C	-	Curie temperature
T_G	-	Glass transition temperature
KG	-	Kilogauss
MUT	-	Material under test
MHz	-	Megahertz
GHz	-	Gigahertz
FM	-	Ferromagnetic
AFM	-	Anti-ferromagnetic
ZFC	-	Zero Field Cool
FC	-	Field Cool
RQF	-	Relative Quality Factor

References

Chapter One

- [1.1] Pond R. Jr. and Maddin R. 1969. *Trans. Met. SOC. ALME* 245, 2475.
- [1.2] Duwez P., Willens R.H. and Klement Jr. W., 1960, *J. Appl. Phys.* 31, 1136.
- [1.3] Mader S. and Nowick A.S., 1965, *Appl. Phys. Lett.* 7, 57.
- [1.4] Tsuei C.C. and Duwez P., 1966, *J. Appl. Phys.* 37, 435.
- [1.5] Simson A.W. and Brambley D.R., 1971, *Phy. Stat. Sol. (b)* 49, 685.
- [1.6] Chi G.C. and Cargill III G.S., *AIP Conf. Proc.* 29, 147(1975)
- [1.7] Luborsky F.F., 1976, *AIP Conf. Proc.* 29, 2009
- [1.8] Egami T., Flenders P.J. and Graham Jr. C.D., 1975a, *AIP Conf. Proc.* 24, 697
- [1.9] Yoshizawa Y. and Yamauchi K. *Mater Sci. Eng. A* 133(1991)176-179
- [1.10] Heinemann K. and Barner K., *Journal of Magnetism and Magnetic Materials* 42(1984)291-294

Chapter Two

- [2.1] Klement Jr. W., Willens R.H., Duwez P.; *Nature*, (1960) 187, 809, ...
- [2.2] Gubanov A.I., 1960, *FIZ. Tel.* 2, 502.
- [2.3] Brenner A., Couchand D.E. and Williams E.K., *J.Res.Nat.Bur.Stand.*44(1950)109
- [2.4] Pond R. Jr. and Maddin R, 1969, *Trans. Met. SOC. ALME* 245, 2475.
- [2.5] Mader S. and Nowick A.S., 1965, *Appl. Phys. Lett.* 7, 57.
- [2.6] Tsuei C.C. and Duwez P., 1966, *J. Appl. Phys.* 37, 435.
- [2.7] Mizoguchi T., *IBM Research Report RC* (1976) 6054.
- [2.8] Alben R, Budnick J.I., Cargil III G.S., *Magnetic Glasses* (American SOC. for Metals. 1978) 304.
- [2.9] Gyorgy E.M., *ibid.* 275.
- [2.10] Cargil III G.S., *Solid State Physics*, Vol. 30 Ed. Ehrenreich et. al., Academic Press, New York (1975) 257.
- [2.11] Masumoto T., Ohnuma S., Shirakawa K., Nose M. and Kobayshi K., *Int. Conf. on Liquid and Amorphous Metals*, Grenoble, France. 1980.
- [2.12] Turnbull D., 1969, *Contemp. Phys.* 10, 473.
- [2.13] Duwez P., Willens R.H. and Klement Jr. W., 1960, *J. Appl. Phys.* 31, 1136.
- [2.14] Chen H.S., *Rep. Prog. Phys.* (1980) 43, 23.

Chapter Three

- [3.1] Pippard A.B., "Magnetoresistance" Cambridge University Press Cambridge UK (1984)
- [3.2] Watts S.M, Wirth S, Von Molnar S, Barry F, and Coey JMD. "Evidence for two-band magnetotransport in half-metallic Chromium oxide", Phys Rev B61, 149621 (2000).
- [3.3] Ashcroft N, and Mermin B. "Solid State Physics" Holt Rinehart and Winston New York (1976).
- [3.4] Harris R., Phischke M. and Zucherman M. "New Model for Amorphous Magnetism" J. Phys. Rev. Lett. Vol. 31(1973) 160.
- [3.5] Polak Ch., Knobel M., Grossinger R., Sato Turtell R.; "The development of nanocrystalline $Fe_{13.5}-Nb_3-Si_{13.5}-B_9$, Magnetism and Structural disorder" J. Magn. Mater. 134(1994) p1

Chapter Four

- [4.1] Scofield J.H., "AC method for measuring low-frequency resistance fluctuation spectra," Review of Scientific Instruments, 58, 985 (1987).
- [4.2] Van der Pauw L.J., "A method of measuring specific resistivity and Hall effects of disks of arbitrary shape", Philips Research Report, 13,1 (1958).

